Shaping Epigenetic Memory via Genomic Bookmarking

Davide Michieletto[1,†,*,‡], Michael Chiang[1,*], Davide Coli[2,*], Argyris Papantonis[3], Enzo Orlandini[2], Peter R. Cook[4], and Davide Marenduzzo[1,†]

[1] *School of Physics and Astronomy, University of Edinburgh, Peter Guthrie Tait Road, Edinburgh, EH9 3FD, UK.*

[2] *Dipartimento di Fisica e Astronomia and Sezione INFN, Universitá di Padova, Via Marzolo 8, Padova 35131, Italy*

[3] *Centre for Molecular Medicine, University of Cologne, Robert-Koch-Str. 21, D-50931, Cologne, DE*

[4] *The Sir William Dunn School of Pathology, South Parks Road, Oxford OX1 3RE, UK.*

∗ *Equal contribution*

† *corresponding author*

‡ *lead contact*

Reconciling the stability of epigenetic landscapes with the rapid turnover of histone modifications and their adaptability to external stimuli is an outstanding challenge. Here, we propose a new biophysical mechanism that can establish and maintain robust yet plastic epigenetic domains via genomic bookmarking (GBM). We model chromatin as a polymer whose segments bear non-permanent histone marks (or "colours") which can be modified by "writer" proteins. The three-dimensional chromatin organisation is mediated by protein bridges, or "readers", such as Polycomb-Repressive-Complexes and Transcription-Factors. The coupling between readers and writers drives spreading of biochemical marks and sustains the memory of local chromatin states across replication and mitosis. On the contrary, GBM-targeted perturbations destabilise the epigenetic landscape. Strikingly, we show that GBM can explain the full distribution of Polycomb marks in a whole Drosophila chromosome. Our model provides a starting point for an understanding of the biophysics of cellular differentiation and reprogramming.

Highlights

- A polymer model with "epigenetic recolouring" and genomic bookmarking (GBM) reconciles rapid turnover of epigenetic marks with stable inheritance of epigenetic landscapes.
- GBM patterns the epigenetic landscape and affects the 3D chromatin organisation. Both are destabilised by GBM-targeted perturbations but unaffected by DNA replication.
- Chromosome-wide simulations employing Polycomb-Response-Elements as examples of GBM recapitulate the distribution of H3K27me3 marks seen in *Drosophila* cells.

INTRODUCTION

Cells belonging to distinct tissues in a multi-cellular organism possess exactly the same genome, yet the DNA sequence is expressed differently. This is made possible by the establishment of lineage-specific epigenetic landscapes – the heritable pattern of post-translational modifications (PTM) on histones and of methylation on DNA [1–8]. Epigenetic landscapes are robust, as they can be "remembered" across many rounds of cell division [1, 2, 7, 9–11]. At the same time, they are plastic and dynamic. They can adapt in response to external stimuli [1, 9, 12–14], and they are affected by disease and ageing [15–17]. Additionally, many biochemical marks encoding the epigenetic information can turn over rapidly and are lost during DNA replication [18, 19]. For example, acetyl groups on histones have half-lives < 10 minutes [18, 20], methyl groups on histones change during the period of one cell cycle [18, 21, 22] and DNA methylation is modified during development [17]. The turnover may originate from histone replacement/displacement during transcription [7, 18, 23], replication [7, 19, 24] or from stochastic PTM deposition and removal [25–27].

Our goal is to develop a biophysical model that can reconcile the reproducible and robust formation of heritable yet plastic epigenetic landscapes across cell populations in the face of the rapid turnover of the underlying histone marks. In particular we will be interested in models which can yield "epigenetic domains", by which we mean 1D stretches of similarly-marked histones which tend to be co-localised and co-regulated [28–32].

Existing models describe changes of PTMs in one-

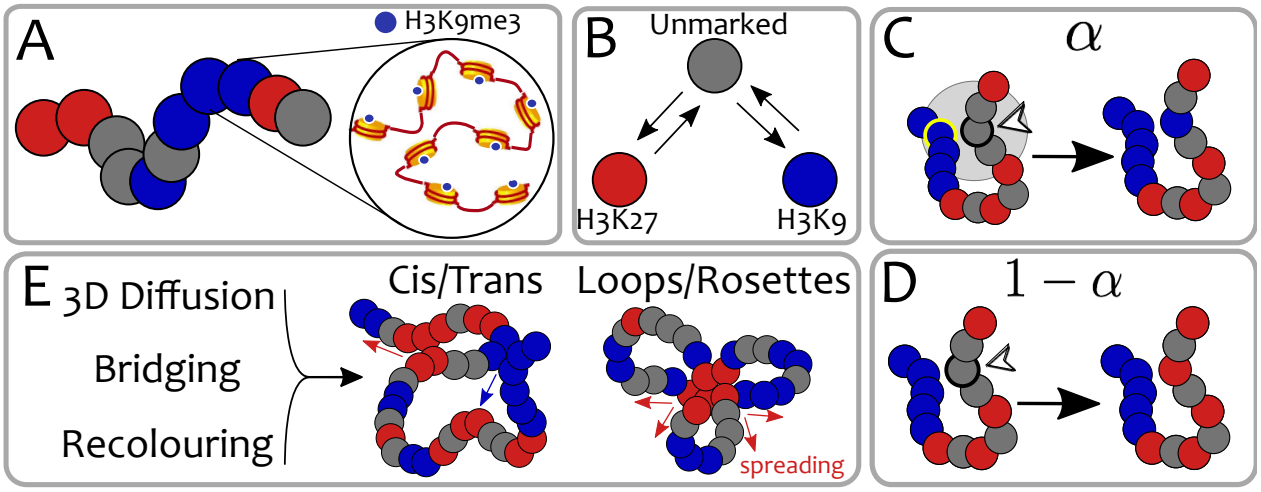

Figure 1. **A Polymer Model for Epigenetic Dynamics.** **(A)** In our coarse-grain polymer model, each bead represents a group of nucleosomes and its colour captures the predominant epigenetic mark. **(B)** Epigenetic marks are dynamic. They can change in between red, blue or grey (no mark) according to biophysical rules. For example, one can think of "red" as an inactive Polycomb state (marked by H3K27me3) or an active acetylated state (marked by H3K27ac) and "blue" as heterochromatic segments (with H3K9me3). The precise nature of the marks does not affect the qualitative behaviour of this generic model. In the Voter-like dynamics, each bead must go through the unmarked state (grey) before changing in the opposite colour [26]. Each bead is selected at rate k_R (see text and SM) and, **(C)** with probability α, it changes its colour "closer" to that of a randomly chosen 3D-proximal bead (in this case the one circled in yellow, see also SM). **(D)** The same bead has probability $1-\alpha$ to undergo a random colour conversion (in this case to red, see SM). **(E)** The synergy between 3D chromatin dynamics, bridging due to (implicit) binding-proteins/TFs and epigenetic recolouring gives rise to dynamical structures such as loop/rosettes and cis/trans contacts which drive (cis and trans) epigenetic spreading (indicated by red/blue arrows, see text).

dimension (1D) or through effective long-range contacts; they yield smooth transitions between stable states and weak (transient) bistability [25, 26, 30, 33–37]. In contrast, our model explicitly takes into account the realistic structure and dynamics of the chromatin fibre in 3D (Fig. **1**) – crucial elements for the spreading of histone marks *in vivo* [11, 38–43].[Note that within the context of our model histone marks, chromatin states and and post-translational histone modifications (PTM) will be used interchangeably.]

From the physical perspective, accounting for realistic 3D interactions (e.g., the formation of loops and trans-contacts driven by the binding of bi- and multi-valent transcription factors) triggers "epigenetic memory" [7, 8], i.e., stability of the epigenetic landscape against extensive perturbations such as DNA replication [7, 44]. Within this framework, the possible "epigenetic phases" of the system are either disordered – no macroscopic epigenetic domain is formed – or homogeneous – only one histone mark spreads over the whole chromosome [44] (see Fig. **2**). Thus, no existing biophysical model can currently predict the spontaneous emergence of multiple heritable epigenetic domains starting from a "blank" chromatin canvas [44].

Here, we propose a model for the *de novo* formation, spreading and inheritance of epigenetic domains that relies solely on three elements. First, we assume a positive feedback between multivalent PTM-binding proteins ("readers") and other proteins which depositing such marks ("writers"). This captures the well-known observations that, for instance, HP1 (a reader binding to heterochromatin) recruits SUV39h1 (a writer for H3K9me3 [45]), and that the Polycomb-Repressive-Complex PRC2 (a reader) contains the enhancer-of-zeste EZH2 (a writer) that spreads H3K27me3 [9, 18, 44, 46, 47]. Second, we assume the presence of genomic bookmarking (GBM) factors, typically transcription factors that can bind to their cognate sites and remain dynamically associated with chromatin through mitosis [48]. Examples of such GBMs include Polycomb-Group-Proteins (PcG) [11, 49–51], and Posterior-Sex-Combs (PSC) [52] bound to Polycomb-Response-Elements (PREs) in *Drosophila* [11, 39, 51, 52], GATA [53, 54] and UBF [55] in humans and Esrbb [56] and Sox2 [48, 57] in mouse. Here, we will use the term transcription factor (TF) to include both activators and repressors. Third, we assume that the recruitment of reading-writing machineries is coupled to specific GBM binding. These three assumptions allow our model to reconcile short-term turnover of PTM with long-term epigenetic memory and plasticity. Our model also quantitatively recapitulates the distribution of H3K27me3 mark seen in Drosophila *in vivo*.

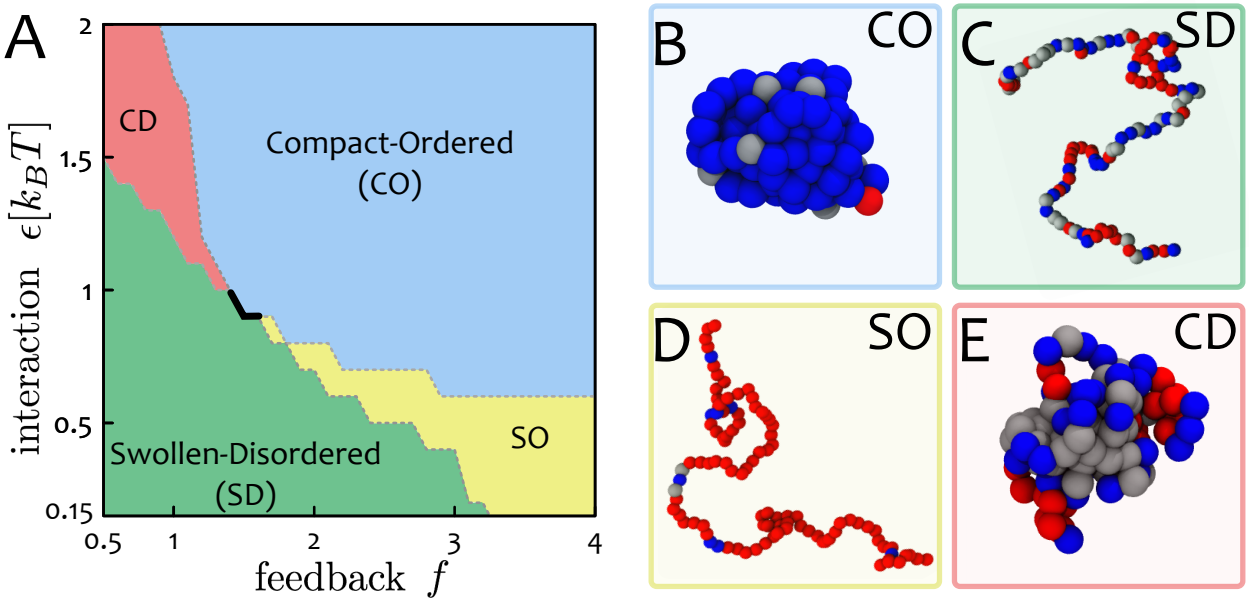

Figure 2. **Phase Diagram: Chromatin States and Epigenetic Memory. (A)** The phase diagram of the system in the space $(\epsilon, f \equiv \alpha/(1-\alpha))$ displays four distinct regions: (i) swollen-disordered (SD); (ii) compact-ordered (CO); (iii) swollen-ordered (SO) and (iv) compact-disordered (CD). The thick solid line represents a first-order transition between the SD and CO phases, whereas the dashed lines signal smoother transitions between the regions. (**B-E**) Representative snapshots of the stable states, which resemble conformations of chromatin seen *in vivo*. The CO phase may be associated to globally-repressed heterochromatin, the SO phase to open transcriptionally-active euchromatin while the CD phase to "gene deserts" characterised by low signal of PTMs and collapsed 3D conformations [28, 29, 58, 59]. The first-order nature of the SD-CO transition entails "epigenetic memory" [8], as the CO phase is robust against extensive perturbations such as the ones occurring during replication [44].

RESULTS

A Polymer Model for Dynamical Epigenetic Landscapes

To capture the dynamic nature of the epigenetic landscape due to PTM turnover, we enhance the (semi-flexible) bead-spring polymer model for chromatin [60–68] by adding a further degree of freedom to each bead. Specifically, each bead – corresponding to one or few nucleosomes (the specific level of coarse-graining does not affect our qualitative results) – bears a "colour" representing the instantaneous local chromatin state (e.g., H3K9me3, H3K27me3, H3K27ac, etc., see Fig. **1**(A)), that can dynamically change in time according to realistic biophysical rules [25, 26, 44]. This is in contrast with previous works [30, 63, 69, 70] that only accounted for static landscapes.

We first consider a toy model in which beads may be found in one of three possible states: grey (unmarked), red (e.g., Polycomb-rich or acetylated) and blue (e.g., heterochromatin-rich). [A more realistic model will be discussed later]. Beads bearing the same histone mark are mutually "sticky", indicating the presence of implicit bridging proteins [18], and can thus bind to each other with interaction energy ϵ. All other interactions are purely repulsive. In addition, we model the action of writer proteins through "recolouring" moves occurring at rate k_R. We choose $k_R = 0.1s^{-1}$, close to typical timescales for acetylation marks [20]. In selected cases, we have also employed a faster recolouring rate of $k_R = 10s^{-1}$ to ensure faster convergence to steady state (see SM for details on simulations and time-mapping).

Our model couples reading and writing as follows. First, a bead is selected randomly. Next, with probability α, it recruits a neighbour from spatially-proximate beads (within $r_c = 2.5\sigma$, where σ is bead size). The colour of the first bead is then shifted one step "closer" to the colour of the second (Fig. **1**B-C). Otherwise (with probability 1-α), the bead undergoes a noisy conversion to one of the other colours (see Fig. **1**D and SM for further details).

This re-colouring scheme encodes a purely non-equilibrium process and it is akin to a "voter" or "infection-type" model [25, 26]. In SM, we describe a "Potts" re-colouring scheme which can be arbitrarily tuned either in- or out-of-equilibrium [44]. Both schemes couple 1D epigenetic information along the chromatin strand to 3D folding. Both drive a positive feedback loop between readers (which bind and bridge chromatin segments) and writers (which can change the underlying epigenetic landscape [18]). Strikingly, both strategies lead to qualitatively similar behaviours, in which cis/trans contacts, globules and rosettes (Fig. **1**E) spontaneously emerge and drive the spread of histone modifications. To simplify the presenta-

tion of our results, and because the observed behaviours are similar, we choose to report in the main text the finding obtained via the "infection-type" model. This model may better capture the one-to-one nature of the chemical reactions required for the deposition (or writing) of histone marks (see SM for more details).

The Phase Diagram of the System Entails Epigenetic Memory

We first map the phase diagram obtained by varying the "feedback" parameter $f = \alpha/(1-\alpha)$ and the attraction energy ϵ/k_BT between any two like-coloured beads. A more realistic model accounting for different attractions between "Polycomb-rich" and "heterochromatin-rich" beads is considered later.

Figure **2**A shows that there are four distinct phases predicted by our minimal model. First, at small α and ϵ/k_BT the fibre is swollen and epigenetically disordered (SD). At large α and ϵ/k_BT, the system is in the compact epigenetically ordered (CO) phase. These two states are separated by a discontinuous transition, signalled by the presence of hysteresis and coexistence (see SM). The discontinuous nature of the transition is important because it confers metastability to the two phases with respect to perturbations. Thus, perturbing a compact heterochromatin-rich state by extensively erasing PTM marks (e.g. during replication) fails to drive the system out of that epigenetic state [44]; in other words, the global epigenetic state is remembered during genome-wide re-organisation events [9, 44].

The two remaining regions of the phase diagram (Fig. **2**A) are (i) an ordered-swollen phase (SO), observed at large α but small or moderate ϵ/k_BT and (ii) a compact-disordered phase (CD), found at small α and large ϵ/k_BT. Our simulations suggest that the transitions from, or to, these states are smooth - unlike that between the SD and CO phases.

Polymer Simulations of the Minimal Model Recapitulate Realistic Chromosome Conformations

Intriguingly, some of the phases in the phase diagram in Fig. **2** correspond to structures seen in eukaryotic chromosomes. Most notably, the compact-ordered phase provides a primitive model for the structure of the inactive copy of the X chromosome in female mammals; this is almost entirely transcriptionally silent, and this state is inherited through many cell divisions [2]. The compact-disordered phase is reminiscent of "gene deserts" (or black chromatin [28, 58]) which have a low concentration of epigenetic marks, and which tend to co-localise in 3D due to self-attraction (possibly mediated by the linker histone H1 [28]). Finally, the swollen ordered phase is reminiscent of open and transcriptionally-active chromatin [59, 71, 72].

In this simplified model, feedback between readers and writers leads to unlimited spreading of a single histone mark in both ordered phases (CO and SO, see Fig. **2**) [44, 73]. Although near-unlimited spreading of silencing marks is seen in telomere position effects in yeast [38] and position-effect variegation in *Drosophila* [74]), this minimal model cannot recapitulate the existence of multiple epigenetic domains – or a "heterogeneous" epigenetic landscape.

A Biophysical Model for Genomic Bookmarking

We now introduce genomic bookmarking (GBM) to account for the coexistence of heritable epigenetic domains, and active/inactive (A/B) compartments [31, 32]. A bookmark is here considered as a TF (activator or repressor) that binds to a cognate site and recruits appropriate readers or writers (see Fig. **3**A).

A mechanistic model of how bookmarks might guide the re-establishment of the previous epigenetic landscape after mitosis remains elusive [17, 48, 54, 75]. Here, we assume that GBMs are expressed in a tissue-specific manner and remain (dynamically) associated to chromatin during mitosis [48, 52]. Then, on re-entering into inter-phase, they can recruit appropriate read/write machineries and re-set the previous transcriptional programme.

In our polymer model, we account for bookmarks by postulating that some of the beads cannot change their chromatin state (Fig. **3**A). Thus, a red (blue) bookmark is a red (blue) bead which cannot change its colour, and otherwise behaves like other red (blue) beads. In Figure **3**A, a bookmark is indicated by an orange square that binds to DNA (rather than a PTM) and recruits read/write machineries (e.g., PRC2), which then spread a histone mark (e.g., H3K27me3) to the neighbours [2, 5, 18, 76]. In our simulations, spreading is driven by the local increase in the density of red-rich (or blue-rich) segments, caused by like-colour attractions as this will increase the probability that at the next re-colouring move a red (blue) mark will be selected, thereby spreading that mark to 3D proximal beads.

GBM Drives the Stable Coexistence of 1D Epigenetic Domains and Shapes the 3D Chromatin Structure

We now consider a chromatin fibre with a fraction ϕ of bookmarks, so the total number of bookmarks is $Q = \phi L$; we analyse how their spatial distribution affects the epigenetic landscape in steady state. We consider three possible GBM distributions, as follows. (i) *Clustered*: Q bookmarks are equally spaced along the fibre; the colour alternates after every n_c consecutive bookmarks ($n_c > 1$ defines the cluster size). (ii) *Mixed:* same as clustered, but

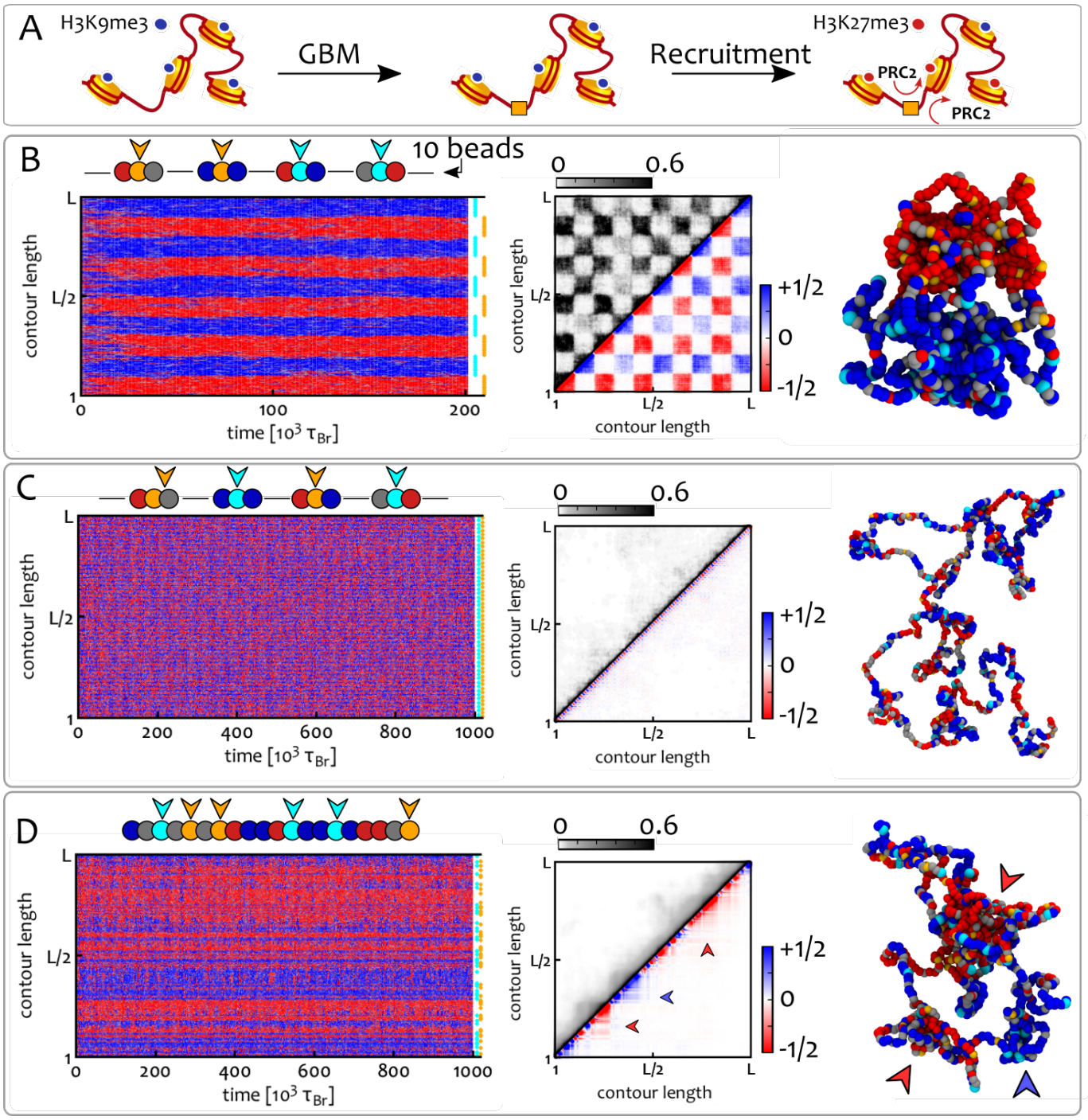

Figure 3. **GBM Shapes the Epigenetic Landscape and Chromatin Conformations.** (**A**) At the nucleosome level, GBM is mediated by a TF that binds to its cognate site and recruits read/write machineries that spread the respective histone mark to 3D-proximal histones (here PRC2 spreads H3K27me3). (**B-D**) We consider a chromatin fibre $L = 1000$ beads long, starting from an epigenetically random and swollen condition with $\phi = 0.1$, equivalent to one bookmark in 150 nucleosomes at 3kbp resolution and we fix $f = 2$ and $\epsilon/k_BT = 0.65$. GBM is modelled by imposing a permanent colour to some beads along the chromatin. Cyan and orange beads denote bookmarks for blue and red marks, respectively. Plots show kymographs (left column), average contact maps (central column) and typical snapshots (right column) for different bookmarking patterns (shown at the end of kymographs and cartoons above). Contact maps are split into two: the upper triangle shows a standard heat-map quantifying the normalised frequency of contacts between segments i and j, whereas the lower triangle shows an "epigenetically-weighted" one in which each contact is weighted by the type of beads involved (+1 for blue-blue contacts, -1 for red-red and 0 for mixed or grey-grey). (**B**) A clustered GBM pattern yields well-defined epigenetic domains which collapse into "A/B-like" compartments ($k_R = 0.1s^{-1}$). (**C**) Alternate GBM maintains the chromosome in a swollen-disordered state ($k_R = 10s^{-1}$). (**D**) Random GBM creates stable and coexisting TAD-like structures which are indicated by the arrowheads ($k_R = 10s^{-1}$).

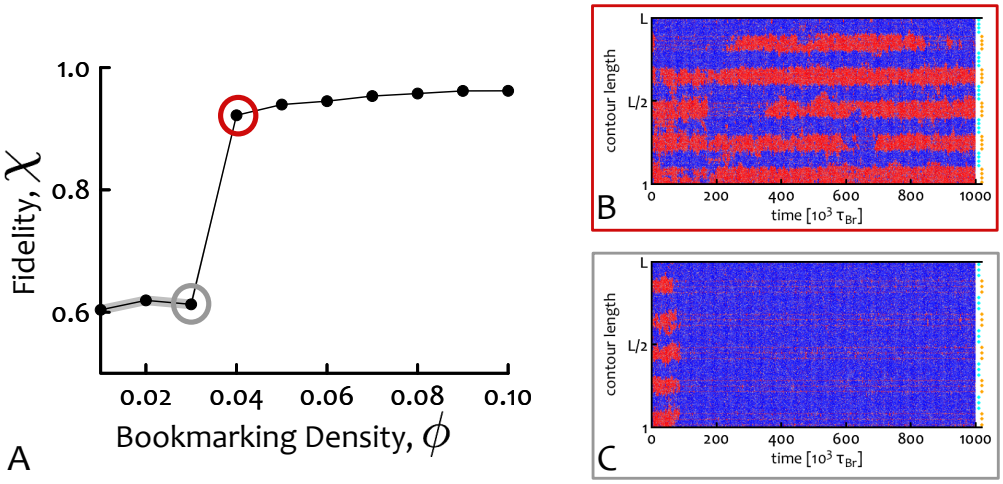

Figure 4. **A Critical Density of Bookmarks is Required for Stable Domain Formation.** (**A**) Using the clustered pattern of bookmarks at different densities ϕ we quantify the deviation from a "perfect" block-like epigenetic landscape. To do this we define the "fidelity", χ, as $1-\Delta^2$ where $\Delta^2 = Var\left[P_{\rm red}(i), \Pi(i)\right]$, i.e. the variance of the probability $P_{\rm red}(i)$ of observing a red bead at position i with respect to the perfect square wave $\Pi(i) = 0.5\left[{\rm sgn}\left(\sin\left(\pi i/n_d\right)\right)+1\right]$, where n_d is the number of beads in a domain (here $n_d = 100$). The fidelity χ jumps abruptly from a value near its lower bound of 1/2 towards unity, at the critical $\phi_c \simeq 0.04$. (**B,C**) Kymographs representing the behaviour of the system at the points circled in red and grey in (**A**).

now colours alternate every other bookmark ($n_c = 1$). (iii) *Random:* bookmarks are placed and colours are chosen randomly along the fibre (ϕ is kept constant).

Figures **3**B-D show the results for $\phi = 0.1$ and a chromatin fibre $L = 1000$ beads long (corresponding to 3 Mbp, or 1.5×10^4 nucleosomes, for a coarse graining of 3 kbp per bead); thus, we assume a fibre with approximately one bookmarked bead every 150 nucleosomes. Simulations are initialised with the chromatin fibre in the swollen disordered phase (non-bookmarked regions contain equal numbers of red, blue and grey beads).

The clustered distribution of bookmarks (Fig. **3**B) quickly reaches a stable epigenetic landscape in which blocks of alternating colours (domains) alternate. On the contrary, the mixed bookmark pattern hinders domain formation, and the fibre remains in the SD state (Fig. **3**C). Remarkably, the random distribution also yields domains in 1D (Fig. **3**D), even in the absence of any correlation between the location of bookmarks.

Importantly, the bookmarking pattern affects 3D structure. Thus, in Figure **3**C-D, both the random and mixed patterns yield swollen or partially-collapsed fibres, even though the parameters used normally drive the system to a collapsed phase. [Note that our parameter choice accounts for the fact that the critical $\epsilon(f)$ marking the SD-CO transition decreases with L.] For the random distribution, the contact map exhibits TAD-like structures, like those found in Hi-C data and long-range interactions between like-coloured domains are strongly suppressed (in contrast to equilibrium models with static epigenetic landscapes [30, 70]). On the other hand, for clustered bookmarks, red and blue domains separately coalesce in 3D (macro-phase-separation), to give a checker-board appearance of the contact map (Fig. **3**B) reminiscent of the patterns found in Hi-C data after suitable normalisation [77].

We suggest that the epigenetic landscape in eukaryotic cells may reflect a subtle combination of clustered and random bookmarking patterns to give local TAD-like structures embedded within a genome globally (micro-)phase-separated into A/B-compartments.

A Critical Density of Bookmarks is Required to Design Stable Domains

We now ask what is the minimum density of like-coloured bookmarks needed to form stable domains.

To address this question we systematically vary bookmark density and perform simulations with clustered patterns (Fig. **3**B) as these are the most effective to create domains. Here, ϕ varies from 0.01 to 0.1 for a chain with $L = 1000$ (i.e., $Q = 10 - 100$). To facilitate the analysis, we fix the domain size at 100 beads (300 kbp), which is in the range of typical HiC domains [31, 32, 77]. Then, there can be a maximum of 10 domains in the simulation (this is achieved by adjusting n_c as ϕ changes). To enhance domain formation, we use $\epsilon/k_BT = 1$, while keeping $f = 2$. To quantify the efficiency of domain formation, we measure the probability that bead i ($1 \le i \le L$) is in a "red" state, $P_{\rm red}(i)$. If ideal regular domains are formed along the fibre (i.e., if all beads have the intended colour, that of the closest bookmarks) then $P_{\rm red}(i)$ would be a perfect square wave $\Pi(i)$ (Fig. **4**, caption). The fidelity of domain formation can then be estimated as $\chi = 1-\Delta^2$, where Δ^2 is the mean

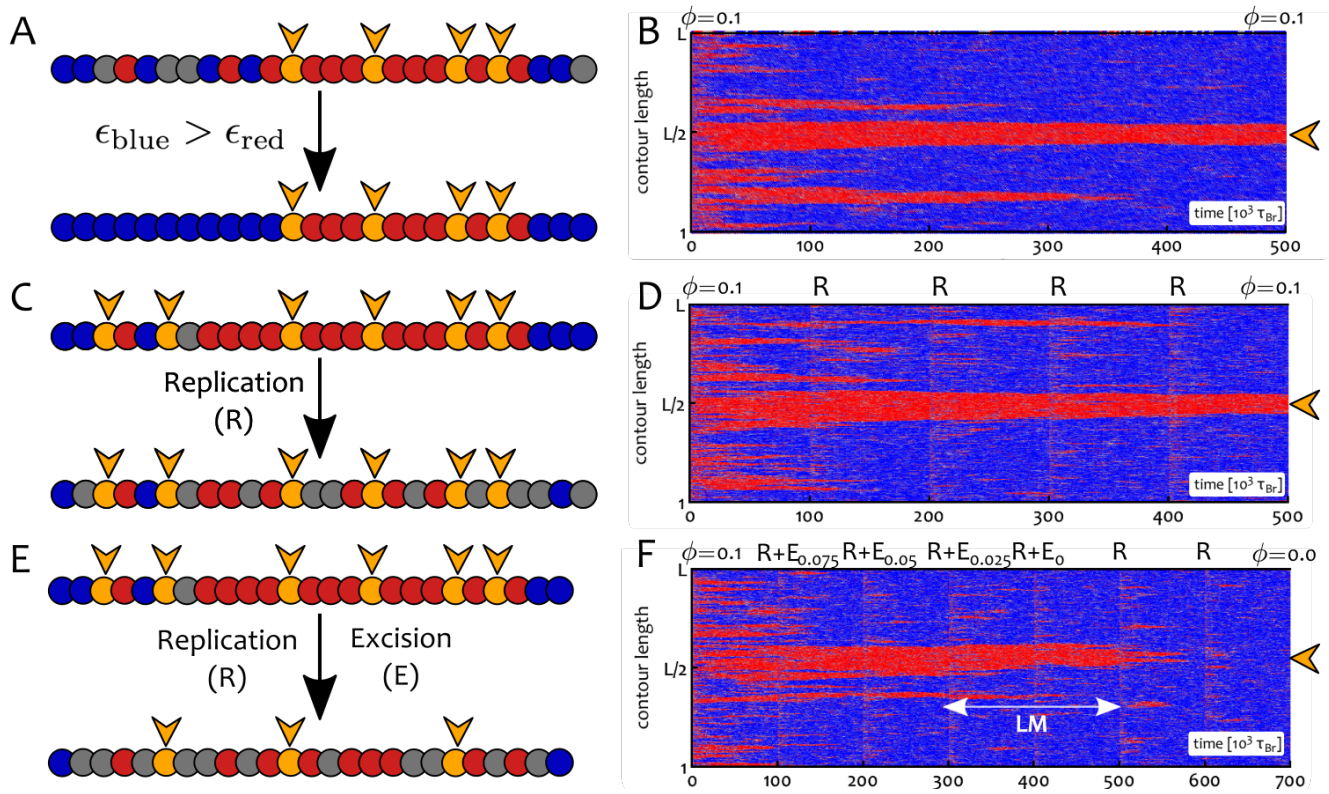

Figure 5. **Asymmetric Interactions and Bookmark Excision but not DNA Replication Affect the Epigenetic Landscape.** (**A-B**) Here we consider the case in which blue-blue interactions are stronger than red-red ones. Specifically, we set $\epsilon_{\rm blue} = 1k_BT$ and $\epsilon_{\rm red} = 0.65k_BT$ with $f = 2$. The central region of a chromatin segment $L = 2000$ beads long is initially patterned with bookmarks at density $\phi = 0.1 > \phi_c$ (the region in the kymograph is indicated by an orange arrowhead). Blue beads invade non-bookmarked regions thanks to the thermodynamic bias whereas the local red state is protected by the bookmarks. (**C-D**) The chromatin fibre undergoes replication cycles which extensively perturb the pattern of PTM of histones on chromatin. A semi-conservative replication event (R) occurs every 10^5 τ_{Br} and half of the (non-bookmarked) beads become grey. The epigenetic landscape is robustly inherited. (**E-F**) The chromatin fibre undergoes semi-conservative replication followed by excision of bookmarks (R+E). At each time, 1/4 of the initial bookmarks are removed and turned into grey (recolourable) beads. The epigenetic landscape is inherited until $\phi < \phi_c$. At this point, the central red domain is either immediately lost (not shown) or it can be sustained through some replication cycles (**F**) by local memory (LM).

square deviation (variance) between $P_{\rm red}(i)$, measured in simulations, and $\Pi(i)$, i.e. $\Delta^2 = \sum_{i=1}^{L} \left[P_{\rm red}(i) - \Pi(i)\right]^2 / L$. The value of $\chi = 1 - \Delta^2$ is low, and approaches 1/2, when the epigenetic landscape is far from the ordered block-like state, and is dominated by a single colour, whereas it tends to unity, for ideal block-like domain formation.

Figure **4**A shows the fidelity of domain formation, χ, as a function of bookmark density, ϕ. As expected from previous results, there is a phase transition at a critical density $\phi_c \simeq 0.04$. For $\phi > \phi_c$, stable domains are seen in kymographs and $\chi \simeq 1$ (see also previous Fig. **3**B). For $\phi < \phi_c$ a single mark takes over the fibre. Near $\phi = \phi_c = 0.04$ there is a sharp transition between these two regimes in which domains appear and disappear throughout the simulation (see kymograph in Fig. **4**B). This critical density may correspond to $1 - 10$ nucleosomes in about 400 as not all nucleosomes in a bookmark bead need to be bookmarked.

Crucially, not all the genome must have this critical density of bookmarks, but only regions required to robustly develop a specific domain of coherent PTM in a given cell-line.

Biasing Stability with Asymmetric Interactions

Thus far, we have considered symmetric interactions between like-coloured beads. In other words, red-red and blue-blue interaction strengths were equal. However, such binding energies may differ if mediated by distinct proteins. Consider the case where red and blue marks encode Polycomb repression and constitutive heterochromatin, respectively. If the blue-blue interaction is larger than the red-red one, the thermodynamic symmetry of the system is broken and the blue mark eventually takes over a non-bookmarked chromatin region (Fig. **5**A). However, if there are bookmarks for the red state, they locally favour the red state, whereas the stronger attraction globally favours the blue mark. This competition creates an additional route

to stable domains as exemplified in Figure **5**A,B. Here, red bookmarks (identified by orange beads) are concentrated in the central segment of a chromatin fibre. Starting from a swollen and epigenetically disordered fibre, where red, blue and grey beads are equal in number, we observe that blue marks quickly invade non-bookmarked regions and convert red beads into blue ones (a process mimicking heterochromatic spreading *in vivo* [45]). However, the central segment containing the bookmarks displays a stable red domain (Fig. **5**A,B).

Bookmark Excision but not DNA Replication Destabilises the Epigenetic Landscape

We next asked whether the epigenetic landscape established through GBM is also stable against extensive perturbations such as DNA replication. In order to investigate this we simulated semi-conservative replication of the chromatin fibre by replacing half of the (non-bookmarked) beads with new randomly coloured beads. In Figure **5**C-D we show that, in agreement with the results of Figures **3** and **4**, our model can "remember" the established epigenetic landscape through multiple rounds of cell division. Importantly, the combination of "memory" [8] and local epigenetic order (via bookmarks) may allow cells to display epialleles with different transcriptional behaviours (local or "cis-" memory [27, 78]).

We next considered a set-up relevant in light of recent experiments in *Drosophila* [51, 79], where the role of PRE in epigenetic memory was investigated. In these works, polycomb-meditated gene repression was perturbed as a consequence of artificial insertion or deletion of Polycomb-Response-Elements (PREs). In Figure **5** we therefore performed a simulated dynamical experiment where replication was accompanied by random excision of bookmarks [51] (Fig. **5**E,F); in practice, we remove 1/4 of the initial number of bookmarks at each replication event. Then each "cell cycle" successively dilutes the bookmarks which at some point can no longer sustain the local red state and the region is consequently flooded with blue marks. Importantly, the system does not display the immediate loss of the red domain as soon as $\phi < \phi_c$; on the contrary, this domain is temporarily retained through local memory [9, 27, 78], which originates from enhanced local density of marks together with the positive read/write feedback (see SM). These results are again consistent with those found experimentally, where regions marked with H3K27me3 are only gradually lost after PRE excision [51].

Chromosome-Wide Simulations Recapitulate Epigenetic Landscapes in *Drosophila*

Simplified models considered thus far are useful to identify generic mechanisms; we now aim to test our model on a realistic scenario. To do so, we perform polymer simulations of the whole right arm of chromosome 3 in *Drosophila* S2 cells.

Bookmarks (orange, in Fig. **6**) are located on the chromosome using PSC ChIP-Seq data [52], as PSC binds to PREs during inter-phase and mitosis [52] as well as recruiting PRC2 (via molecular bridging). Some other beads are permanently coloured according to the "9-state" Hidden Markov Model (HMM, [58]). If they correspond to gene deserts (state 9), promoter/enhancers (state 1) or transcriptionally active regions (states 2-4) they are coloured grey, red and green, respectively. We further introduce an interaction between promoter and enhancer beads to favour looping, plus, an attractive interaction between gene desert (grey) beads mimicking their compaction by H1 linker histone [28] (see SM for full list of parameters). The remaining 20% of the polymer is left blank and these "unmarked" beads are allowed to dynamically change their chromatin state into heterochromatin (blue) or polycomb (purple) according to our recolouring scheme.

We evolve the system to steady state and we evaluate the probability of finding a Polycomb mark at a certain genomic position [80]. This provides us with an *in silico* ChIP-seq track for polycomb marks which can be compared with *in vivo* ChIP-Seq data [58] (see Fig. **6**B). The two are in good agreement (Pearson correlation coefficient $\rho = 0.46$, against $\rho = 0.006$ for a random dataset).

Remarkably, not all bookmarked segments (orange) are populated by Polycomb marks; instead we observe that H3K27me3 spreading requires appropriate 3D folding (Fig. **6**B-C, insets). Bookmarks which do not contact other bookmarks due to the local epigenetic landscape do not nucleate H3K27me3 spreading. Again, this is consistent with 3D chromatin conformation being crucial for the spreading and establishment of epigenetic landscapes [11, 40, 43].

DISCUSSION

We proposed and investigated a new biophysical mechanism for the *de novo* establishment of epigenetic domains and their maintenance through interphase and mitosis. Our simplest model requires only one element: a positive feedback between readers (e.g., binding proteins HP1, PRC2, etc.) and writers (e.g., methyltransferases SUV39, EzH2, etc.).

We performed large-scale simulations in which chromatin is modelled as a semi-flexible bead-and-spring polymer chain [60–62, 66] overlaid with a further degree of freedom representing the dynamic epigenetic landscape [44, 73]. Specifically, each bead is assigned a colour corresponding to the local instantaneous epigenetic state (e.g., unmarked, polycomb- or acetylation-rich (red) and heterochromatin-rich (blue)). Readers are implicitly included by setting an attraction between like-coloured beads [63, 70], whereas writers are modelled by perform-

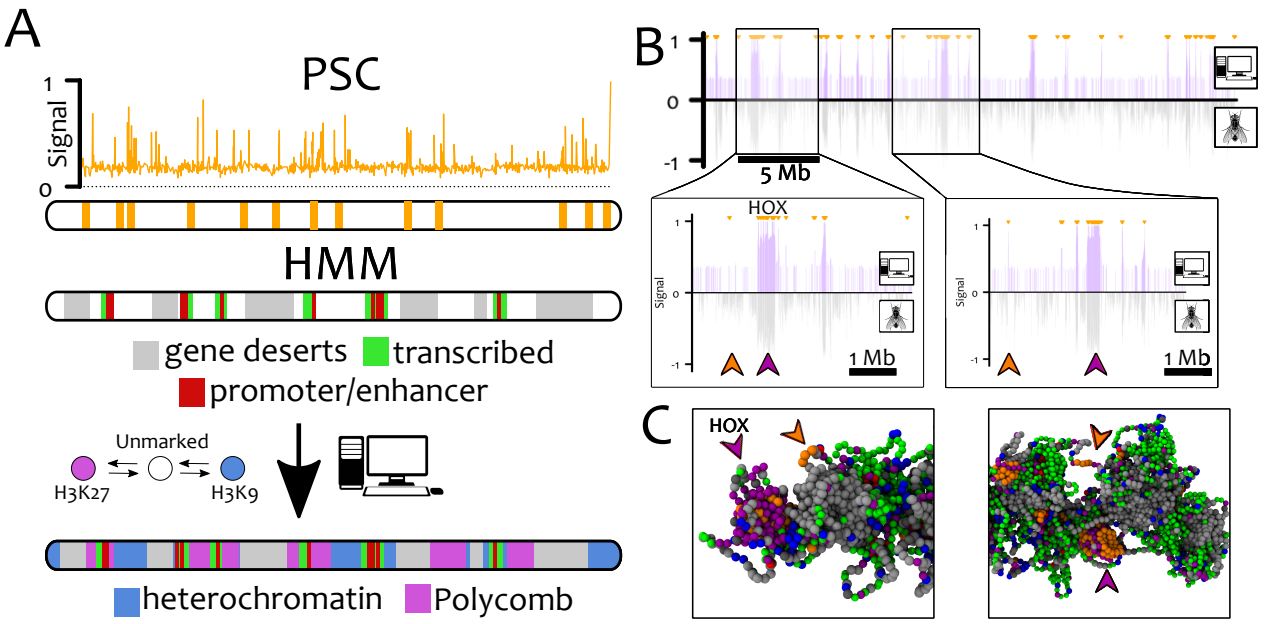

Figure 6. **GBM is Sufficient to Recapitulate the Distribution of Polycomb Marks in *Drosophila* S2 cells.** In this figure, we apply our GBM model to a realistic scenario: We perform chromosome-wide simulations of Ch3R of Drosophila S2 cells at 3 kbp resolution ($L = 9302$). (**A**) The location of PSC/PRE bookmarks are mapped onto beads using ChIP-Seq data [52]. Using results from the "9-states" HMM [58], gene deserts (regions lacking any mark in ChIP-seq data, state 9), promoter/enhancers (state 1) and transcriptionally active regions (states 2-4) are permanently coloured grey, red and green, respectively. The remaining beads are initially unmarked (white) and may become either heterochromatin (states 7,8 – blue) or polycomb (state 6 – purple). (**B**) *In silico* ChIP-seq data for H3K27me3 (top half, purple lines) is compared with *in vivo* ChIP-seq [58] (bottom half, grey line). Small orange arrow at the top of the profile indicate the location of the bookmarks. The excellent quantitative agreement between the datasets is captured by the Pearson correlation coefficient which is $\rho = 0.46$ – to be compared with $\rho = 0.006$ obtained between a random and the experimental datasets. We highlight that not all the bookmarked beads foster the nucleation of H3K27me3 domain (see big purple/orange arrowheads in the insets, corresponding to the HOX cluster). The reason can be found by analysing the 3D conformations of the chromosome (**C**). The non-nucleating bookmarks (orange arrowheads), although near in 1D, are found far from potential target beads in 3D space (purple arrowheads) and so fail to yield large H3K27me3 domains.

ing re-colouring moves according to realistic and out-of-equilibrium rules [26, 34] (see Fig. **1**). Intriguingly, we note that the main qualitative behaviours are retained when detailed balance is restored [44] (see SI).

If read-write positive feedback is sufficiently strong, a single histone mark can spread through an epigenetically "disordered" fibre to induce a discontinuous transition to a collapsed-ordered state (see Fig. **2**). The dominant histone mark is either the one corresponding to the strongest 3D attraction (Fig. **5**) or is selected by spontaneous symmetry-breaking if 3D attractions are equal (Fig. **2**). The compact-ordered structure is stable: even if some beads lose their colour, their neighbours can restore it quickly. This "epigenetic memory" renders our chromatin model robust against extensive perturbations, such as those occurring during replication [5, 18, 38], when most histones are removed or displaced [2, 18].

The main limitation of this simple model is that epigenetic order in real chromosomes is local, rather than global. Multiple epigenetic domains – each with one mark – coexist on a chromosome [32], thereby forming an "heterogeneous" epigenetic landscape. Our main result is that our model predicts the formation of heterogeneous epigenetic landscapes which can be inherited when we include genomic bookmarking (GBM).

Bookmarks are usually considered to be transcription factors that remain (dynamically) associated through mitosis so gene activity can be inherited from one interphase to the next [54, 57, 75]. We envisage bookmarks perform an additional function which is typical of many TFs: they recruit read/write machineries, and hence nucleate the spreading of epigenetic marks and the establishment of epigenetic domains. Here we assumed bookmarking TFs are permanently bound to DNA, however our conclusions should hold even for dynamic bookmarks that switch between bound and unbound state [48, 81].

Stable domains can be formed with only one type of bookmark, when the competing histone mark is thermodynamically favoured (Fig. **5**). This result rationalises the common understanding that heterochromatin can spread at lengths (blue mark in Fig. **5**A,B) and it is stopped by actively transcribed (bookmarked) regions. Further, it is in agreement with recent genome editing experiments in *Drosophila*: when PRE is inserted into the genome, it pro-

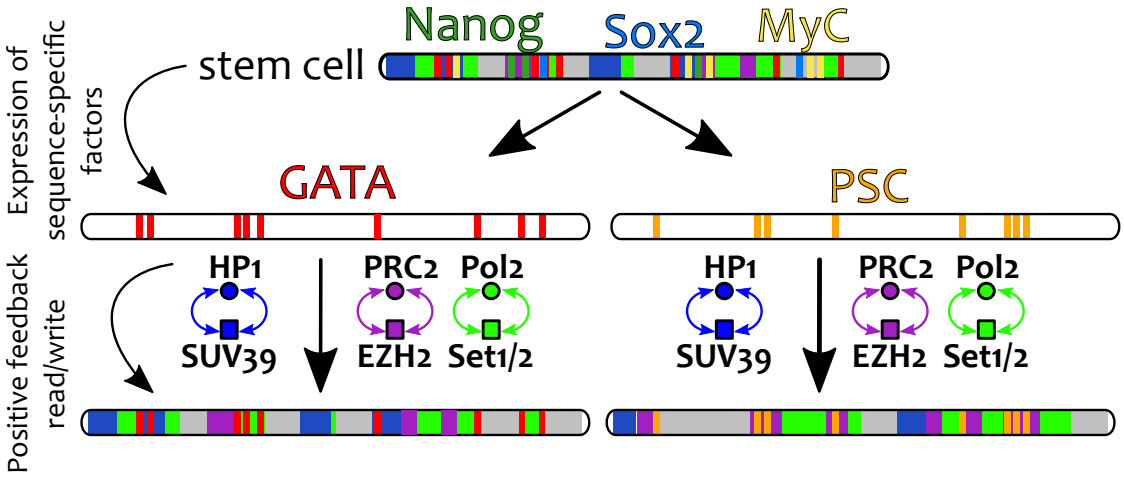

Figure 7. **Model for Cellular Differentiation**. We speculate that cellular differentiation may be driven by a two-step process. First, sequence-specific factors (bookmarks) are expressed as a consequence of environmental and positional cues. Second, the positive feedback set up by read/write machineries drives the establishment and maintenance of tissue-specific epigenetic landscapes. As a consequence, genomic bookmarks are key targets to understand cellular differentiation and reprogramming.

vides a bookmark for H3K27me3 which leads to spreading of that mark [51], whereas PRE excision leads to (gradual) loss of the mark [51]. These findings can be readily explained within our model if the 3D attraction between polycomb marks is slightly weaker than that between, e.g., H3K9me3-modified regions (Fig. **5**). Additionally, the expression of HOX and other Polycomb-regulated genes (which contain multiple PREs) is less sensitive to deletion of single PREs [82]. We suggest that this is because domains remain stable as long as bookmark density is kept above the critical threshold (Fig. **4**).

Our results thus strongly suggest that bookmarks are key elements that allow cells to access and maintain the correct "memory" of the previous epigenetic landscapes. Losing bookmarks (via artificial excision or DNA mutation) will thus impair the ability of cells to inherit the cell-line-specific epigenetic landscape. In addition, we argue that newly activated bookmarks (for instance subsequently to inflammation response or external stimuli [13, 14, 83]) may drive the *de novo* formation of transient epigenetic domains which allow the plastic epigenetic response to environmental changes.

Our model also recreates the pattern of H3K27me3 in *Drosophila* S2 cells. Here, GBM by PSC leads to epigenetic spreading within a pattern of active TFs, and inactive gene deserts. Besides being quantitatively accurate, our simulations show that not all PRE bookmarks end up in H3K27me3 domains: whether or not they do, depends on their network of chromatin contacts in 3D, as highlighted experimentally in [11, 40, 43]. This is also reminiscent of the well-known position effect according to which the activity of a gene depends on its local environment [14].

Our results also prompt several further questions. First, starting from a stem cell, how might different cell lineages be established? We suggest that environmental and morphological cues trigger production of lineage-specific bookmarks such as GATA [54] and PSC [52], which trigger the positive feedback between readers and writers to generate and sustain new epigenetic landscapes (Fig. **7**). Thus, bookmarks are here envisaged as key elements that should be targeted in order to understand, and manipulate, cellular differentiation. Second, how might reprogramming factors like Sox2, Nanog, and Myc work? Possibly, their binding generates alternative feedback cycles that mask [15] the action of pre-existing bookmarks, thereby allowing other bookmarks to establish new epigenetic landscapes.

We have extended the existing notion of GBM [54, 57, 75, 84] to include the direct recruitment of read/write machineries. This coupling allows our model to predict the *de novo* establishment of heterogeneous epigenetic landscapes which can be remembered across replication and can adapt to GBM-targeted perturbations.

Within our framework, architectural elements such as CTCF [2], Cohesins [61] and SAF-A [72] may provide the initial 3D chromatin conformation upon which the GBM-driven establishment of epigenetic landscape takes place [11, 40, 43].

Author Contribution

D.Mi.,A.P.,E.O.,P.R.C. and D.Ma. designed research and discussed results. D.Mi.,M.C.,D.C. performed simulations. All authors wrote the paper.

Acknowledgements

We acknowledge the European Research Council for funding (Consolidator Grant THREEDCELLPHYSICS,

Ref. 648050). Work in the Papantonis lab is supported by CMMC core funding. The authors thank C. A. Brackley, A. Buckle, N. Gilbert and J. Allan for insightful remarks on the manuscript.

[1] C. H. Waddington, Nature **150**, 563 (1942).
[2] B. Alberts, A. Johnson, J. Lewis, D. Morgan, and M. Raff, *Molecular Biology of the Cell* (Taylor & Francis, 2014) p. 1464.
[3] B. Strahl and C. Allis, Nature **403**, 41 (2000).
[4] T. Jenuwein and C. D. Allis, Science **293**, 1074 (2001).
[5] G. Cavalli and T. Misteli, Nat. Struct. Mol. Biol. **20**, 290 (2013).
[6] B. Pal, T. Bouras, W. Shi, F. Vaillant, J. M. Sheridan, N. Fu, K. Breslin, K. Jiang, M. E. Ritchie, M. Young, G. J. Lindeman, G. K. Smyth, and J. E. Visvader, Cell Rep. **3**, 411 (2013).
[7] A. V. Probst, E. Dunleavy, and G. Almouzni, Nat. Rev. Mol. Cell. Biol. **10**, 192 (2009).
[8] R. K. Ng and J. B. Gurdon, Nat. Cell Biol. **10**, 102 (2008).
[9] A. Angel, J. Song, C. Dean, and M. Howard, Nature **476**, 105 (2011).
[10] A. Kouskouti and I. Talianidis, EMBO J. **24**, 347 (2005).
[11] F. Ciabrelli, F. Comoglio, S. Fellous, B. Bonev, M. Ninova, Q. Szabo, A. Xuéreb, C. Klopp, A. Aravin, R. Paro, F. Bantignies, and G. Cavalli, Nat. Genet. (2017).
[12] S. Stern, Y. Fridmann-Sirkis, E. Braun, and Y. Soen, Cell Rep. **1**, 528 (2012).
[13] S. Wood and A. Loudon, J. Endocrinol. **222** (2014).
[14] A. Feuerborn and P. R. Cook, Trends Genet. **31**, 483 (2015).
[15] A. Zirkel, M. Nikolic, K. Sofiadis, J.-P. Mallm, L. Brant, C. Becker, J. Altmueller, J. Franzen, M. Koker, E. G. Gusmao, I. G. Costa, R. T. Ullrich, W. Wagner, P. Nuernberg, K. Rippe, and A. Papantonis, bioRxiv **144** (2017).
[16] S. Pal and J. Tyler, Sci. Adv. **2**, 253 (2016).
[17] E. Heard and R. A. Martienssen, Cell **157**, 95 (2014).
[18] G. E. Zentner and S. Henikoff, Nat. Struct. Mol. Biol. **20**, 259 (2013).
[19] A. Klosin, K. Reis, C. Hidalgo-Carcedo, E. Casas, T. Vavouri, and B. Lehner, Sci. Adv. **3** (2017), 10.1126/sciadv.1701143.
[20] T. K. Barth and A. Imhof, Trends Biochem. Sci. **35**, 618 (2010).
[21] T. B. Kheir and A. H. Lund, Essays Biochem. **48**, 107 (2010).
[22] C. Alabert, T. K. Barth, N. Reverón-Gómez, S. Sidoli, A. Schmidt, O. Jensen, A. Imhof, and A. Groth, Genes Dev. **29**, 585 (2015).
[23] P. J. Skene and S. Henikoff, Development **140**, 2513 (2013).
[24] A. N. D. Scharf, T. K. Barth, and A. Imhof, Nucleic Acids Res. **37**, 5032 (2009).
[25] C. Arnold, P. F. Stadler, and S. J. Prohaska, J. Theor. Biol. **336**, 61 (2013).
[26] I. B. Dodd, M. A. Micheelsen, K. Sneppen, and G. Thon, Cell **129**, 813 (2007).
[27] S. Berry, C. Dean, and M. Howard, Cell Syst. **4**, 445 (2017).
[28] T. Sexton, E. Yaffe, E. Kenigsberg, F. Bantignies, B. Leblanc, M. Hoichman, H. Parrinello, A. Tanay, and G. Cavalli, Cell **148**, 458 (2012).
[29] J. R. Dixon, S. Selvaraj, F. Yue, A. Kim, Y. Li, Y. Shen, M. Hu, J. S. Liu, and B. Ren, Nature **485**, 376 (2012).
[30] D. Jost, P. Carrivain, G. Cavalli, and C. Vaillant, Nucleic Acids Research **42**, 1 (2014).
[31] S. S. P. Rao, M. H. Huntley, N. C. Durand, E. K. Stamenova, I. D. Bochkov, J. T. Robinson, A. L. Sanborn, I. Machol, A. D. Omer, E. S. Lander, and E. L. Aiden, Cell **159**, 1665 (2014).
[32] J. R. Dixon, I. Jung, S. Selvaraj, Y. Shen, J. E. Antosiewicz-Bourget, A. Y. Lee, Z. Ye, A. Kim, N. Rajagopal, W. Xie, Y. Diao, J. Liang, H. Zhao, V. V. Lobanenkov, J. R. Ecker, J. A. Thomson, and B. Ren, Nature **518**, 331 (2015).
[33] M. A. Micheelsen, N. Mitarai, K. Sneppen, and I. B. Dodd, Phys. Biol. **7**, 026010 (2010).
[34] I. B. Dodd and K. Sneppen, J. Mol. Biol. **414**, 624 (2011).
[35] L. C. M. Anink-Groenen, T. R. Maarleveld, P. J. Verschure, and F. J. Bruggeman, Epigenetics chromatin **7**, 30 (2014).
[36] M. J. Obersriebnig, E. M. H. Pallesen, K. Sneppen, A. Trusina, and G. Thon, Nat. Commun. **7**, 11518 (2016).
[37] F. Erdel and E. C. Greene, Proc. Nat. Acad. Sci. USA **113**, E4180 (2016).
[38] P. B. Talbert and S. Henikoff, Nat. Rev. Genet. **7**, 793 (2006).
[39] C. Lanzuolo, V. Roure, J. Dekker, F. Bantignies, and V. Orlando, Nat. Cell Biol. **9**, 1167 (2007).
[40] J. M. Engreitz, A. Pandya-jones, P. Mcdonel, A. Shishkin, K. Sirokman, C. Surka, S. Kadri, J. Xing, A. Goren, E. S. Lander, K. Plath, and M. Guttman, Science **341**, 1 (2013).
[41] S. F. Pinter, R. I. Sadreyev, E. Yildirim, Y. Jeon, T. K. Ohsumi, M. Borowsky, and J. T. Lee, Genome Res. **22**, 1864 (2012).
[42] T. Schauer, Y. Ghavi-Helm, T. Sexton, C. Albig, C. Regnard, G. Cavalli, E. E. Furlong, and P. B. Becker, EMBO reports (2017).
[43] W. Deng, J. W. Rupon, I. Krivega, L. Breda, I. Motta, K. S. Jahn, A. Reik, P. D. Gregory, S. Rivella, A. Dean, and G. A. Blobel, Cell **158**, 849 (2014).
[44] D. Michieletto, E. Orlandini, and D. Marenduzzo, Phys. Rev. X **6**, 041047 (2016).
[45] N. A. Hathaway, O. Bell, C. Hodges, E. L. Miller, D. S. Neel, and G. R. Crabtree, Cell **149**, 1447 (2012).
[46] S. Hauri, F. Comoglio, M. Seimiya, M. Gerstung, T. Glatter, K. Hansen, R. Aebersold, R. Paro, M. Gstaiger, and C. Beisel, Cell Rep. **17**, 583 (2016).
[47] A. Collinson, A. J. Collier, N. P. Morgan, A. R. Sienerth, T. Chandra, S. Andrews, and P. J. Rugg-Gunn, Cell Rep. **17**, 2700 (2016).
[48] S. S. Teves, L. An, A. S. Hansen, L. Xie, X. Darzacq, and R. Tjian, Elife **5**, 1 (2016).
[49] J. A. Kassis and J. L. Brown, Advances in genetics **81**, 83 (2013).
[50] B. Schuettengruber, N. Oded Elkayam, T. Sexton, M. Entrevan, S. Stern, A. Thomas, E. Yaffe, H. Parrinello, A. Tanay, and G. Cavalli, Cell Rep. **9**, 219 (2014).
[51] F. Laprell, K. Finkl, and J. Müller, Science **8266**, eaai8266 (2017).
[52] N. E. Follmer, A. H. Wani, and N. J. Francis, PLoS Genet. **8** (2012).
[53] S. Kadauke, M. I. Udugama, J. M. Pawlicki, J. C. Achtman, D. P. Jain, Y. Cheng, R. C. Hardison, and G. A. Blobel, Cell **150**, 725 (2012).

[54] S. Kadauke and G. A. Blobel, Epigenetics chromatin **6**, 6 (2013).

[55] A. Grob, C. Colleran, and B. McStay, Genes Dev. **28**, 220 (2014).

[56] N. Festuccia, A. Dubois, S. Vandormael-Pournin, E. G. Tejeda, A. Mouren, S. Bessonnard, F. Mueller, C. Proux, M. Cohen-Tannoudji, and P. Navarro, Nat. Cell Biol. **18**, 1139 (2016).

[57] C. Deluz, E. T. Friman, D. Strebinger, A. Benke, M. Raccaud, A. Callegari, M. Leleu, S. Manley, and D. M. Suter, Genes Dev. **30**, 2538 (2016).

[58] P. V. Kharchenko, A. A. Alekseyenko, Y. B. Schwartz, A. Minoda, N. C. Riddle, J. Ernst, P. J. Sabo, E. Larschan, A. A. Gorchakov, T. Gu, D. Linder-Basso, A. Plachetka, G. Shanower, M. Y. Tolstorukov, L. J. Luquette, R. Xi, Y. L. Jung, R. W. Park, E. P. Bishop, T. K. Canfield, R. Sandstrom, R. E. Thurman, D. M. MacAlpine, J. A. Stamatoyannopoulos, M. Kellis, S. C. R. Elgin, M. I. Kuroda, V. Pirrotta, G. H. Karpen, and P. J. Park, Nature **471**, 480 (2011).

[59] N. Gilbert and W. A. Bickmore, Biochem. Soc. Symp. **73**, 59 (2006).

[60] A. Rosa and R. Everaers, PLoS Comp. Biol. **4**, 1 (2008).

[61] G. Fudenberg, M. Imakaev, C. Lu, A. Goloborodko, N. Abdennur, and L. A. Mirny, Cell Rep. **15**, 2038 (2016).

[62] L. A. Mirny, Chromosom. Res. **19**, 37 (2011).

[63] C. A. Brackley, J. Johnson, S. Kelly, P. R. Cook, and D. Marenduzzo, Nucleic Acids Res. **44**, 3503 (2016).

[64] C. A. Brackley, D. Michieletto, F. Mouvet, J. Johnson, S. Kelly, P. R. Cook, and D. Marenduzzo, Nucleus **7**, 453 (2016).

[65] C. A. Brackley, S. Taylor, A. Papantonis, P. R. Cook, and D. Marenduzzo, Proc. Natl. Acad. Sci. USA **110**, E3605 (2013).

[66] T. M. Cheng, S. Heeger, R. A. Chaleil, N. Matthews, A. Stewart, J. Wright, C. Lim, P. A. Bates, and F. Uhlmann, Elife **4**, 1 (2015).

[67] A. L. Sanborn, S. S. P. Rao, S.-C. Huang, N. C. Durand, M. H. Huntley, A. I. Jewett, I. D. Bochkov, D. Chinnappan, A. Cutkosky, J. Li, K. P. Geeting, A. Gnirke, A. Melnikov, D. McKenna, E. K. Stamenova, E. S. Lander, and E. L. Aiden, Proc. Natl. Acad. Sci. USA **112**, 201518552 (2015).

[68] A. Rosa, N. B. Becker, and R. Everaers, Biophys. J. **98**, 2410 (2010).

[69] M. Di Pierro, B. Zhang, E. L. Aiden, P. G. Wolynes, and J. N. Onuchic, Proc. Natl. Acad. Sci. USA **113**, 201613607 (2016).

[70] M. Barbieri, M. Chotalia, J. Fraser, L.-M. Lavitas, J. Dostie, A. Pombo, and M. Nicodemi, Proc. Natl. Acad. Sci. USA **109**, 16173 (2012).

[71] N. Gilbert, S. Gilchrist, and W. A. Bickmore, Int. Rev. Cytol. **242**, 283 (2004).

[72] R.-S. Nozawa, L. Boteva, D. C. Soares, C. Naughton, A. R. Dun, B. Ramsahoye, P. C. Bruton, R. S. Saleeb, M. Arnedo, B. Hill, R. Duncan, S. K. Maciver, and N. Gilbert, Cell (2017).

[73] D. Michieletto, E. Orlandini, and D. Marenduzzo, arXiv:1705.03226 , 1 (2017).

[74] G. Schotta, A. Ebert, V. Krauss, A. Fischer, J. Hoffmann, S. Rea, T. Jenuwein, R. Dorn, and G. Reuter, EMBO J. **21**, 1121 (2002).

[75] K. D. Sarge and O. K. Park-Sarge, Trends Biochem. Sci. **30**, 605 (2005).

[76] T. Cheutin and G. Cavalli, PLoS Genet. **8** (2012).

[77] E. Lieberman-Aiden, N. L. van Berkum, L. Williams, M. Imakaev, T. Ragoczy, A. Telling, I. Amit, B. R. Lajoie, P. J. Sabo, M. O. Dorschner, R. Sandstrom, B. Bernstein, M. A. Bender, M. Groudine, A. Gnirke, J. Stamatoyannopoulos, L. A. Mirny, E. S. Lander, and J. Dekker, Science **326**, 289 (2009).

[78] S. Berry, M. Hartley, T. S. G. Olsson, C. Dean, and M. Howard, Elife **4**, 1 (2015).

[79] R. T. Coleman and G. Struhl, Science **8236**, 10.1126/science.aai8236 (2017).

[80] To determine these probability, a bookmarked bead is counted as bearing the H3K27me3 mark when it is near beads with polycomb marks, or within large stretches of bookmarked beads.

[81] C. A. Brackley, B. Liebchen, D. Michieletto, F. Mouvet, P. R. Cook, and D. Marenduzzo, Biophys J. **112**, 1085 (2017).

[82] S. De, A. Mitra, Y. Cheng, K. Pfeifer, and J. A. Kassis, PLoS Genet. **12**, 1 (2016).

[83] I. Kirmes, A. Szczurek, K. Prakash, I. Charapitsa, C. Heiser, M. Musheev, F. Schock, K. Fornalczyk, D. Ma, U. Birk, C. Cremer, and G. Reid, Genome Biol. **16**, 246 (2015).

[84] J. M. Caravaca, G. Donahue, J. S. Becker, X. He, C. Vinson, and K. S. Zaret, Genes Dev. **27**, 251 (2013).

Shaping Epigenetic Memory via Genomic Bookmarking: Supplementary Information

D. Michieletto[1,†,*], M. Chiang[1,*], D. Coli[2,*], A. Papantonis[3], E. Orlandini[2], P. R. Cook[4], and D. Marenduzzo[1,†]
[1] *School of Physics and Astronomy, University of Edinburgh, Peter Guthrie Tait Road, Edinburgh, EH9 3FD, UK.*
[2] *Dipartimento di Fisica e Astronomia and Sezione INFN, Universitá di Padova, Via Marzolo 8, Padova 35131, Italy*
[3] *Centre for Molecular Medicine, University of Cologne, Robert-Koch-Str. 21, D-50931, Cologne, DE*
[4] *The Sir William Dunn School of Pathology, South Parks Road, Oxford OX1 3RE, UK.*
∗ *Equal contribution*
† *corresponding author*

SIMULATION DETAILS

We first discuss the simulation methods and additional results associated with the "Voter-" or "infection-"like model that is mentioned in the main text. We then present an alternative recolouring strategy, the "Potts" model. Both recolouring schemes produce qualitatively similar results but we favour the infection-type model (and we report it in the main text) as it is fundamentally an out-of-equilibrium model and better captures the common notion of one-to-one chemical reactions that underlie the deposition of epigenetic marks on chromatin and histones. The "Potts" recolouring scheme models recolouring of the segments by computing the effective change in energy after a recolouring move (as explained below) and therefore it is a "many-to-one" type of reaction.

VOTER-LIKE MODEL

We model the chromatin fibre as a semi-flexible bead-spring chain of M beads. Each bead has a diameter of $\sigma = 30$ nm and represents roughly 3 kbp, which corresponds to around 15 nucleosomes. Each bead is also assigned a "colour" q to represent a particular epigenetic modification (or mark). Apart from the *Drosophila* simulation, we assume that there are three colours ($q \in \{1, 2, 3\}$), which can generally be viewed as an active, unmodified, and inactive epigenetic mark respectively.

We simulate the dynamics of the chromatin fibre by performing molecular dynamics (MD) simulations in Brownian scheme: we only model explicitly the interactions between the monomers of the fibre, but we include a stochastic force on each monomer to implicitly account for the random collisions between the (much smaller) solvent particles and the monomers.

As commonly conducted in MD simulations, we express properties of the system in multiples of fundamental quantities. Energies are expressed in units of k_BT, where k_B is the Boltzmann constant and T is the temperature of the solvent. Distances are expressed in units of σ, which, as defined above, is the diameter of the bead. Further, time is expressed in units of the Brownian time τ_{Br}, which is the typical time for a bead to diffuse a distance of its size – more precisely, $\tau_{Br} = \sigma^2/D$, where D is the diffusion constant for the bead.

The interactions between the beads are governed by several potentials that are standard in polymer physics. First, there is a purely repulsive (Weeks-Chandler-Anderson) potential acting between consecutive beads to reduce overlapping:

$$U^{ab}_{WCA}(r) = k_BT\left[4\left[\left(\frac{\sigma}{r}\right)^{12} - \left(\frac{\sigma}{r}\right)^{6}\right] + 1\right](\delta_{b,a+1}+\delta_{b,a-1}) \tag{1}$$

if $r < 2^{1/6}\sigma$ and 0 otherwise, where r is the separation between the two beads. Second, there is a finite extensible nonlinear elastic (FENE) spring between consecutive beads to ensure chain connectivity:

$$U^{ab}_{FENE}(r) = -\frac{K_f R_0^2}{2}\ln\left[1 - \left(\frac{r}{R_0}\right)^2\right](\delta_{b,a+1} + \delta_{b,a-1}), \tag{2}$$

where R_0 (set to 1.6σ) is the maximum separation between beads and K_f (set to $30k_BT/\sigma^2$) is the strength of the spring. The combination of the WCA and FENE potential with the chosen parameters gives a bond length that is approximately equal to σ [1]. Third, we model the stiffness of the chromatin via a Kartky-Porod term:

$$U^{ab}_{KP} = \frac{k_BTl_p}{\sigma}\left[1 - \frac{\boldsymbol{t}_a \cdot \boldsymbol{t}_b}{|\boldsymbol{t}_a|\,|\boldsymbol{t}_b|}\right](\delta_{b,a+1} + \delta_{b,a-1}), \tag{3}$$

where $\boldsymbol{t}_a$ and $\boldsymbol{t}_b$ are the tangent vectors connecting bead a to $a+1$ and b to $b+1$ respectively; l_p is the persistent length of the chain and is set to $3\sigma \approx 100$ nm, which is within the range of values estimated from experiments and computer simulations [2]. Last, to model the effect of a bridging protein, or "reader", binding to multiple sites along the chromatin fibre with the same epigenetic mark, we include a truncated and shifted Lennard-Jones (LJ) potential that acts between beads which are not immediate neighbours of

each other (i.e. not between bead a and $a+1$):

$$U_{LJ}^{ab}(r) = 4\epsilon_{q_a q_b}\left[\left(\frac{\sigma}{r}\right)^{12} - \left(\frac{\sigma}{r}\right)^{6} - \left(\frac{\sigma}{r_c^{q_a q_b}}\right)^{12} + \left(\frac{\sigma}{r_c^{q_a q_b}}\right)^{6}\right] \cdot (1-\delta_{b,a+1})(1-\delta_{b,a-1}) \quad (4)$$

if $r \leq r_c^{q_a q_b}$ and 0 otherwise. When the beads have different colours, or when one or more of the beads are unmodified (i.e. $q_a \neq q_a$, or q_a or $q_b = 2$), we set $\epsilon_{q_a q_b} = k_B T$ and $r_c^{q_a q_b} = 2^{1/6}\sigma$ to model pure repulsion between the beads. When both beads are modified and have the same colour ($q_a = q_b$ and $q_a, q_b \neq 2$), we set $\epsilon_{q_a q_b} = \epsilon\, k_B T$ and $r_c^{q_a q_b} = r_c > 2^{1/6}\sigma$ to model attraction caused by the "reader". The length r_c sets the cut-off distance, or the maximum distance that a modified bead will feel an attraction from another bead with the same colour. It corresponds to the effective interaction distance of the "reader" with the chromatin. We choose $r_c = 2.5\sigma$ for the attractive force between beads to be effective. The parameter ϵ governs the strength of the attraction between like-colour beads. It is one of the parameters which we vary in the simulation to explore the possible configurations of the fibre.

To summarise, the total potential energy related to bead a is the sum of all the pairwise and triplet potentials involving the bead:

$$U_a = \sum_{b \neq a} \left(U_{WCA}^{ab} + U_{FENE}^{ab} + U_{KP}^{ab} + U_{LJ}^{ab}\right). \quad (5)$$

The time evolution of each bead along the fibre is governed by a Brownian dynamics scheme with the following Langevin equation:

$$m_a \frac{d^2 \boldsymbol{r}_a}{dt^2} = -\nabla U_a - \gamma_a \frac{d\boldsymbol{r}_a}{dt} + \sqrt{2k_B T \gamma_a}\boldsymbol{\eta}_a(t), \quad (6)$$

where m_a and γ_a are the mass and the friction coefficient of bead a, and $\boldsymbol{\eta}_a$ is its stochastic noise vector obeying the following statistical averages:

$$\langle \boldsymbol{\eta}(t) \rangle = 0; \quad \langle \eta_{a,\alpha}(t)\eta_{b,\beta}(t') \rangle = \delta_{ab}\delta_{\alpha\beta}\delta(t-t'), \quad (7)$$

where the Latin indices represent particle indices and the Greek indices represent Cartesian components. The last term of Eq. 6 represents the random collisions caused by the solvent particles. For simplicity, we assume all beads have the same mass and friction coefficient (i.e. $m_a = m$ and $\gamma_a = \gamma$). We also set $m = \gamma = k_B = T = 1$. The Langevin equation is integrated using the standard velocity-Verlet integration algorithm, which is performed using the Large-scale Atomic/Molecular Massively Parallel Simulator (LAMMPS) [3]. For the simulation to be efficient yet numerically stable, we set the integration time step to be $\Delta t = 0.01\,\tau_{Br}$, where τ_{Br} is the Brownian time as mentioned previously.

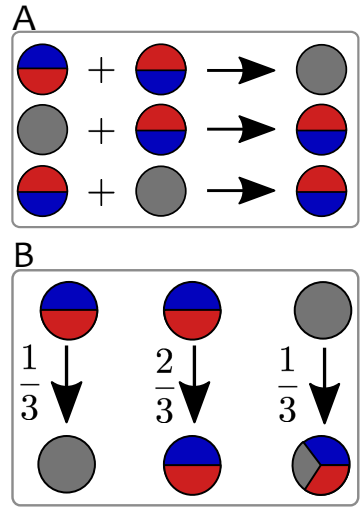

Fig. S **1**. Conversion rules for (**A**) recruited re-colouring or (**B**) random (noisy) re-colouring according to the "Voter-" or "infection-"like scheme [4]. The generic types of epigenetic marks are 1="red" (acetylated or polycomb rich), 2="grey" (unmarked) and 3="blue" (heterochromatin rich).

Voter-Like Recolouring Scheme

We recolour the beads based on the 1D model proposed in [4]. As discussed in the main text, we consider two recolouring rates: (i) a faster recolouring rate $k_R = 10\,\mathrm{s}^{-1}$ for steady-state measurements and (ii) a slower rate $k_R = 0.1\,\mathrm{s}^{-1}$ for observing transient dynamics. In each recolouring step, we conduct M (M is the number of beads making up the polymer) attempts of colour conversion such that each bead, on average, receives a single conversion attempt. The procedure of a specific conversion attempt is as follows:

1. A bead n_1 to be modified is first selected from the fibre. It either undergoes a recruited conversion attempt (Step 2), with probability α, or a noisy conversion attempt (Step 3), with probability $1-\alpha$.

2. Recruited conversion: Another bead n_2 is selected at random from the beads that are within the cut-off distance $r_c = 2.5\sigma$ from n_1. The colour of n_1 is then changed one step towards that of n_2. More precisely, the rules are as follows (see Fig. S**1A**):

   - If $q_{n_2} = 1$, q_{n_1} is changed $3 \to 2$ or $2 \to 1$
   - If $q_{n_2} = 3$, q_{n_1} is changed $1 \to 2$ or $2 \to 3$
   - If $q_{n_2} = 2$ or $q_{n_1} = q_{n_2}$, q_{n_1} remains the same

3. Noisy conversion: n_1 is changed one step towards either one of the two other states with probability of 1/3, and no direct conversion between $q = 1$ and 3 is allowed. Specifically, the rules are as follows (see Fig. S**1B**):

- If $q_{n_1} = 1$ or 3, it has a probability of 1/3 switching to 2 and a probability of 2/3 remaining the same
- If $q_{n_1} = 2$, it has an equal probability of 1/3 switching to any of the states

This rule ensures that there is, on average, an equal number of beads in each of the three states when the probabilities of a recruited conversion and a noisy one are the same ($\alpha = 1 - \alpha = 0.5$).

The recolouring rules do not allow the direct conversion between $q = 1$ and 3. This is to model that any existing modifications have to be de-modified before another modification can be applied, in line with the observations that there are de-modifying enzymes (HDACs and HDMs) and modifying enzymes (HATs and HMTs). The recruited conversion represents the positive feedback mechanism suggested in the main text, where a "reader" enzyme for a particular epigenetic mark tends to attract a "writer" enzyme of the same mark. On the other hand, the noisy conversion simulates the activity of free modifying and de-modifying enzymes that change the modifications along the fibre in a stochastic manner.

The key parameter which governs the epigenetic landscape in this recolouring scheme is the ratio of the probability of a recruited attempt to that of a noisy attempt, $f = \alpha/(1-\alpha)$, which is referred as the feedback parameter. It is clear that a higher f would give a higher probability for a recruited conversion to occur, resulting in a stronger feedback and a more coherent landscape. This ratio is the other parameter that is varied in the simulation to alter the configuration of the chromatin fibre.

Initial Conditions and Equilibration

We simulate the chromatin fibre inside a periodic cube with a linear dimension L. To avoid self-interactions through the periodic boundaries, we set the box size to be much larger than the volume occupied by the chromatin: $L = 100\sigma$ for a chain of $M \leq 500$ beads; $L = 150\sigma$ for $500 < M \leq 2000$; and $L = 220\sigma$ for the *Drosophila* simulation.

As with any molecular dynamics simulations, the initial conditions of the system are important to consider. We initialise the chromatin fibre as an ideal random walk chain with each bead having a random epigenetic colour (i.e. a swollen, epigenetically disordered configuration). We run the simulation for $10^4\,\tau_{Br}$ to equilibrate the fibre, during which the beads only interact via steric repulsion (along with the usual potentials to maintain chain connectivity and stiffness) and epigenetic interactions are switched off. In particular, we employ a soft potential to remove any cross-links and overlaps in the polymer for the first $10\,\tau_{Br}$ such that it becomes a self-avoiding chain. In formula, the potential is given by

$$U^{ab}_{soft}(r) = \begin{cases} A\left[1 + \cos\frac{\pi r_{ab}}{r_c}\right] & \text{for } r < r_c \\ 0 & \text{otherwise,} \end{cases} \tag{8}$$

with $r_c = 2^{1/6}\sigma$ is the cut-off distance and A is the maximum of the potential, which is set to $100k_BT$. This potential has the advantage that it remains bound as r_{ab} goes to zero and, therefore, does not generate numerical divergence when pushing the monomers apart. We revert to the WCA potential, as specified in Eq. 1 (but acting between any beads), for the remaining time of the equilibration period.

Mapping between Simulation and Physical Units

We provide here a possible mapping between the quantities measured in the simulation and their physical counterparts for comparing the simulation results with experimental data. Energies measured in the simulation can be mapped easily by multiplying by the relevant temperature (e.g. $T \sim 300$ K) and the Boltzmann constant. Distances can also be mapped in a similar manner by substituting a physical value for the diameter of a bead σ (e.g. $\sigma = 30$ nm). Mapping simulation time to physical time requires a more careful analysis. As mentioned above, simulation time is expressed in units of the Brownian time τ_{Br}, which is related to the diffusion constant D of a bead by the formula $\tau_{Br} = \sigma^2/D$. The diffusion constant is also given by the Einstein relation

$$D = \frac{k_BT}{\gamma} = \frac{k_BT}{3\pi\eta\sigma}, \tag{9}$$

where we have assumed that each bead diffuses like a sphere and applied Stoke's law, with η being the viscosity of the fluid that the fibre is submerged in. Hence, we obtain the following expression of the Brownian time in terms of measurable quantities:

$$\tau_{Br} = \frac{3\pi\eta\sigma^3}{k_BT}. \tag{10}$$

As discussed in [1], if the nucleoplasm has a viscosity $\eta \sim 10$ cP, one Brownian time maps to approximately 1 ms. A simulation of $10^6\,\tau_{Br}$ therefore corresponds to ~ 16 min in real life.

First-Order-Like Transition between SD and CO Phase

As mentioned in the main text, the model exhibits a sharp, first-order-like transition between the swollen, epigenetically disordered (SD) and the compact, epigenetically ordered (CO) phase. This order of transition is signified by the presence of coexistence and hysteresis near the

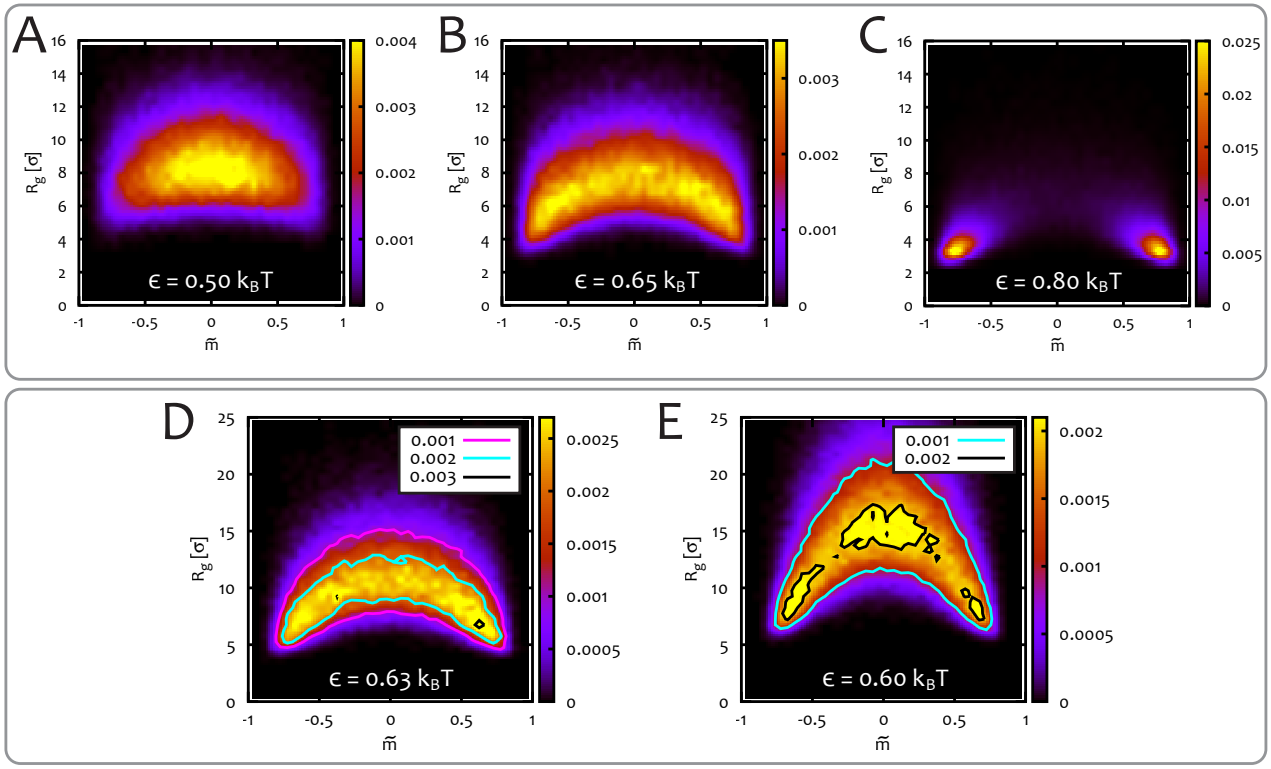

Fig. S **2**. Top panel: Joint-probability distribution $P(R_g, \widetilde{m})$ for a modelled chromatin with $M = 100$ beads for three ϵ values, corresponding to the case in which the system is (**A**) in the SD phase, (**B**) at the transition point, and (**C**) in the CO phase. The feedback is $f = 2$ in all three cases. Each probability distribution is produced from sampling the system's configurations in 100 simulations. Bottom panel: Joint probability distribution at the transition point for two different system sizes: (**D**) $M = 200$ and (**E**) $M = 400$. Contour lines are plotted to highlight the variation in the probability values. These diagrams show the emergence of three peaks as the system size increases, indicating phase coexistence. Each distribution is produced from sampling 100 simulations, except for the case $M = 400$ in which 200 samples were considered.

phase boundary. We identify these characteristics from studying the phase of the polymer in the parameter space (ϵ, f) using two order parameters: (i) the radius of gyration (R_g) for compactness of the fibre:

$$R_g^2(t) = \frac{1}{M} \sum_{a=1}^{M} \left(\boldsymbol{r}_a(t) - \langle \boldsymbol{r}(t) \rangle\right)^2 , \tag{11}$$

where $\boldsymbol{r}_a(t)$ is the position of bead a at time t and $\langle \boldsymbol{r} \rangle$ is the mean position of the chain; (ii) a (signed) epigenetic "magnetisation" for coherence of the epigenetic colour:

$$\widetilde{m}(t) = \frac{1}{M} \left[N_b(q = 3, t) - N_b(q = 1, t)\right] , \tag{12}$$

where $N_b(q, t)$ is the number of beads with colour q at time t. We also consider the absolute value of this quantity:

$$m(t) = \frac{1}{M} \left|N_b(q = 3, t) - N_b(q = 1, t)\right| , \tag{13}$$

which is useful for distinguishing the epigenetically disordered phase ($m \sim 0$) and ordered phase ($m \sim 1$).

We study the transition between the SD and CO phase by varying the interaction energy ϵ between like-colour beads while fixing the feedback at $f = 2$. Figure S**2** reports the joint probability distribution $(P_(R_g, \widetilde{m}))$ of the system with a particular radius of gyration and (signed) magnetisation. For a chain with $M = 100$ beads, we show the distribution for the case when it is in the SD phase, at the transition point, and in the CO phase (Fig. S**2A**-**C**). The distribution at the transition point indicates that the probability of finding the system in both SD and CO phases are similarly probable, but so as any intermediate states between the two phases. As we increase the length of the polymer (i.e. $M = 200$ and $M = 400$, Fig. S**2D** and **E**), three peaks begin to emerge for the distribution at the transition point (top peak for the SD phase and bottom two peaks for the CO phase), providing further evidence of phase coexistence.

Such coexistence is further confirmed when we demonstrate that the system exhibits hysteresis near the transition point, which is another hallmark of a first-order transition. Fig. S**3** presents the results of a set of simulations conducted to test the presence of hysteresis. In these sim-

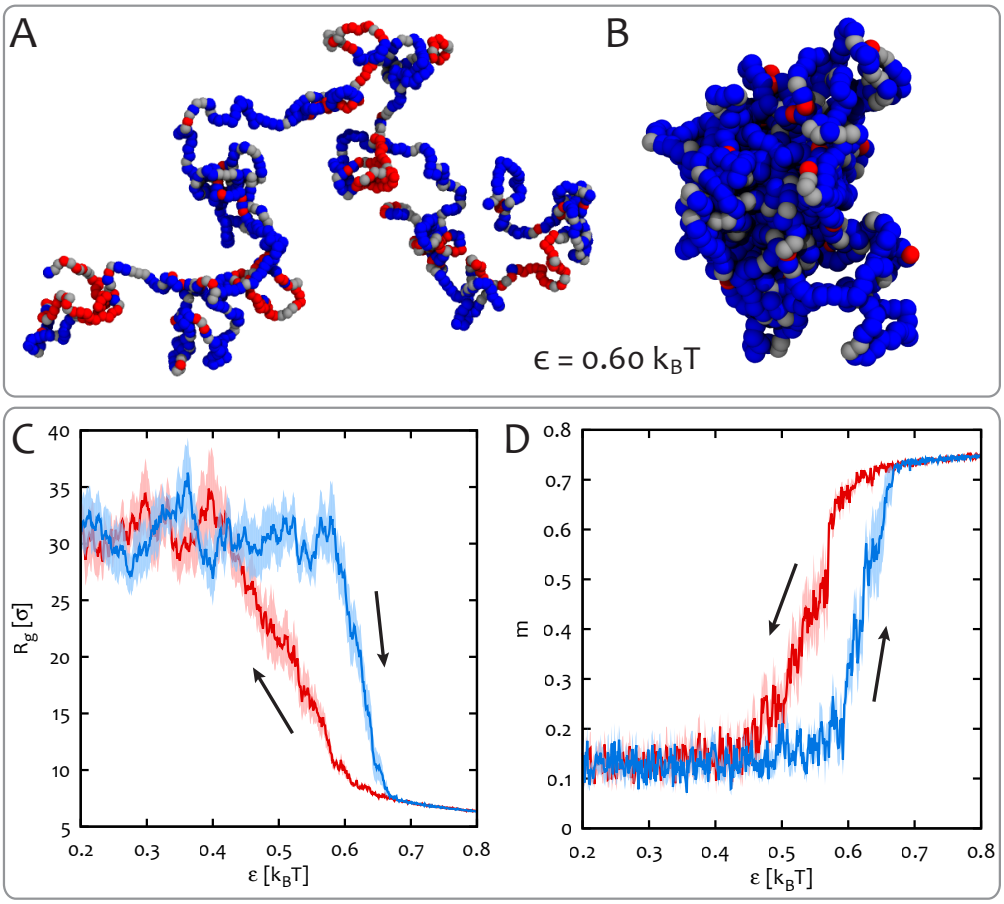

Fig. S **3**. Simulation results indicating the presence of coexistence and hysteresis near the phase boundary with $f = 2$. The top panel shows snapshots of coexisting phases ((**A**) SD and (**B**) CO) observed at $\epsilon = 0.6$. The bottom panel shows the measured (**C**) radius of gyration R_g and (**D**) magnetisation m when ϵ is varied slowly, first from 0.8 to 0.2 (red curve) and then in the opposite direction (blue curve) ($1.5 \times 10^6\ \tau_{Br}$ in each direction). Both figures show a small region of hysteresis cycle between $\epsilon \sim 0.58 - 0.62$. The curves in the figures represent averages over 10 simulations, and the shaded region indicates the standard error of the mean.

ulations, we initialise the chromatin fibre with $M = 1000$ beads to a CO configuration with $\epsilon = 0.8$. We slowly reduce ϵ to 0.2 (in decrements of 0.001) such that the system changes from a CO to a SD configuration. Once at $\epsilon = 0.2$, the inverse process is performed. Under this procedure, we observe that there is a small interval $\epsilon \sim 0.58 - 0.62$ in which the system can be in either phases depending on its configurational history (Fig. S**3C**, **D**). For example, at $\epsilon = 0.6$, the chain is compact and ordered when reducing ϵ, but it is swollen and disordered when increasing ϵ (Fig. S**3A**, **B**). These observations provide a strong evidence that hysteresis and coexistence are present in this transition.

Drosophila Simulation

In the *Drosophila* simulation, we employ a more realistic epigenetic colour scheme. We reserve a separate colour for the heterochromatin (HET), polycomb, unmarked regions, actively transcribed regions, promoters, gene deserts, and bookmarked (PSC) segments. The energies for the interactions which are not purely repulsive are summarised in Table I. The initial colouring of the polymer is detailed in the main text.

Interaction	**Energy** $[k_BT]$
polycomb - polycomb	0.60
HET - HET	0.72
PSC - PSC	0.90
polycomb - PSC	0.90
gene desert - gene desert	0.60
promoter - promoter	3.00
promoter - transcribed	0.60
transcribed - transcribed	0.60

Table S I. Energies for non-repulsive interactions in the *Drosophila* simulation

"POTTS" MODEL

In this section, we describe the alternative recolouring scheme we adopt in the "Potts" model, and present some results using this recolouring scheme. Below we also describe the molecular dynamics potentials we used in this model. This recolouring strategy is the same used in Ref. [5].

The fiber is modelled using a semi-flexible bead and spring chain. Each bead is marked with a Potts-state $q = \{1, 2, 3\}$ which respectively stands for three possible epigenetic states. The dynamics of this chain is then described by a set of Langevin equations at the temperature T_L. At rate τ_R^{-1}, we modify the colour of the beads using Metropolis moves at the temperature T_R. After time τ_R all the beads have been typically attempted to be recoloured once. This process is then repeated several times (typically 1000), until steady state is reached.

Molecular Dynamics Potentials

We can generally describe the dynamics of a chain composed of M beads of mass m of size σ, employing an Hamiltonian H in the form:

$$H = \sum_{i=1}^{M} \frac{1}{2} m \left(\frac{\mathrm{d}\boldsymbol{r}_i}{\mathrm{d}t} \right)^2 + U\left(\{\boldsymbol{r}_i\}_{i=1\ldots M}, \{q_i\}_{i=1\ldots M} \right) \ , \tag{14}$$

where the first term is the kinetic one, while the second is a general interaction term between beads. In our case, we model the interactions as follows:

$$U = \mathrm{U_H}\left(\boldsymbol{r}\right) + \mathrm{U_{KP}}\left(\boldsymbol{r}\right) + \mathrm{U_{LJ}^{tot}}\left(\boldsymbol{r}, q\right) \ , \tag{15}$$

where:

i) $\mathrm{U_H}$ is an harmonic interaction which ensures the connectivity of the chain:

$$\frac{1}{k_B T_L} \mathrm{U_H}(\{\boldsymbol{r}_i\}_{i=1\ldots M}) = \sum_{i=1}^{M-1} \frac{k_h}{2 k_B T_L} \left(\|\boldsymbol{r}_i - \boldsymbol{r}_{i+1}\| - r_0 \right)^2 \ . \tag{16}$$

ii) $\mathrm{U_{KP}}$ is a Kratky-Porod term which models the stiffness of the chain:

$$\frac{1}{k_B T_L} \mathrm{U_{KP}}\left(\{\boldsymbol{r}_i\}_{i=1\ldots M}\right) = \frac{\ell_P}{2\sigma} \sum_{i=1}^{M-2} \left(1 - \frac{\boldsymbol{u}_i \cdot \boldsymbol{u}_{i+1}}{\|\boldsymbol{u}_i\| \, \|\boldsymbol{u}_{i+1}\|} \right) \ , \tag{17}$$

where $\boldsymbol{u}_j \equiv \boldsymbol{r}_{j+1} - \boldsymbol{r}_j$ and $\frac{1}{2}\ell_P$ is usually identified with the persistence length of the chain.

iii) $\mathrm{U_{LJ}^{tot}}$is the total contribute to the energy of the bead-bead interaction. Generally we write:

$$\mathrm{U_{LJ}^{tot}}\left(\boldsymbol{r}_{i=1\ldots M}, q_{i=1\ldots M}\right) = \sum_{j>i} U_{\mathrm{LJ}}(\|\boldsymbol{r}_i - \boldsymbol{r}_j\|; q_i, q_j) \ , \tag{18}$$

with U_{LJ} being a truncated and shifted Lennard-Jones potential in the following form:

$$\begin{aligned} \beta_L U_{\mathrm{LJ}}(r; q_i, q_j) = & \frac{4}{\mathcal{N}} \frac{\varepsilon(q_i, q_j)}{k_B T_L} \left[\left(\frac{\sigma}{r}\right)^{12} - \left(\frac{\sigma}{r}\right)^{6} + \right. \\ & \left. - U_0(r_c(q_i, q_j)) \right] \Theta\left(r - r_c(q_i, q_j)\right) \ , \end{aligned} \tag{19}$$

where Θ is the Heaviside step function and U_0 is an auxiliary function which ensures that $U_{\mathrm{LJ}}(r_c(q_i, q_j); q_i, q_j) \equiv 0$. The cutoff $r_c(q_i, q_j)$ models the interaction between the various possible epigenetic marks, we set:

(a) $r_c(q_i, q_j) = 2^{1/6}\sigma$ if $q_i \neq q_j$ or $q_i = q_j = 3$, modeling only steric interaction between beads with different epigenetic marks or unmarked ($q = 3$);

(b) $r_c(1, 1) = r_c(2, 2) = 1.8\sigma$, modeling the effective attractive interaction between beads with the same epigenetic marks mediated by the "readers" enzymes.

Finally, the free parameter $\varepsilon(q_i, q_j)$ is:

$$\frac{\varepsilon(q_i, q_j)}{k_B T_L} = \begin{cases} \epsilon / k_B T_L & \text{if } q_j = q_j = \{1, 2\} \\ 1 & \text{otherwise} \end{cases} \tag{20}$$

and $\mathcal{N}$ is a parameter which ensures that the minimum of the attractive part is $-\epsilon / k_B T_L$.

For our convenience, we define the parameters $\alpha_L \equiv \epsilon / k_B T_L$ and $\alpha_R \equiv \epsilon / k_B T_R$.

Detailed Balance

One of the main feature of the Potts model is that it permits to study both the equilibrium and the non-equilibrium dynamics of the system. The model is in equilibrium when $\alpha_R = \alpha_L$ whereas it break detailed balance (and therefore it is a non-equilibrium model) when $\alpha_R \neq \alpha_L$.

We now prove our previous statement using a Kolmogorov loop through some states of the system: Let us consider four different possible states A,B,C,D:

A two beads are close and have the same (non-unmarked) epigenetic mark;

B two beads are close and have different epigenetic mark;

C two beads are far from each other and have different epigenetic mark;

D two beads are far from each other and have the same (non-unmarked) epigenetic mark.

We now estimate the probability of doing the cycle $A \to B \to C \to D \to A$ using Metropolis-like moves; if the system is at an equilibrium regime, this probability will be equal to the probability of the inverse cycle $A \to D \to C \to B \to A$.

The first move $A \to B$ is the only one of the cycle which involves an energy loss in the system; since this move is a recolouring one, we conclude that probability it occurs is $p(A \to B) \sim e^{-\alpha_R}$. As already mentioned, the other moves do not involve energy loss, hence we conclude that the probability of our cycle goes like:

$$p(A \to B \to C \to D \to A) \sim e^{-\alpha_R} \ .$$

We can compute the probability of the inverse cycle in the same way. The only move which involves energy loss is the first one $D \to A$ which this times is connected with the Langevin dynamics of the system. We can therefore conclude that:

$$p(A \to D \to C \to B \to A) \sim e^{-\alpha_L} \ .$$

This shows that probabilities of the two cycles are equal if and only if $\alpha_R = \alpha_L$.

Simulation Details

Numerical simulations are performed using the software LAMMPS[3]. We study the dynamics of chains composed of M beads of mass $m = 1$ and size $\sigma = 1$. The dynamics is studied in a diluted regime: we place the chains inside a cubic container of side $L = 100\sigma$ with reflecting boundary conditions at border (volume fraction for $M = 1000$ is $\approx 0.4\%$). The spatial configuration of the chain evolves via a Langevin dynamics with damping parameter γ derived by the Hamiltonian (14). We employed the parameters:

$$k_h = 200\epsilon \qquad r_0 = 2^{1/6}\sigma \qquad \ell_P = 3\sigma \qquad \gamma = 1\tau_{LJ}^{-1} \ .$$

Numerical integrations of the Langevin equations are then performed using the LAMMPS engine [3].

Recolouring dynamics takes place every 10^5 timesteps ($\tau_R = 10^3\ \tau_{Br}$). At each recolouring step we perform a number $N_R = M$ (where M is the number of beads making up the polymer) Metropolis moves at temperature T_R.

To quantify the configurations of the polymer, we employ two different order parameters: the gyration radius R_g and the mean magnetisation m, defined as:

$$R_g^2 = \frac{1}{M}\sum_{i=1}^{M}\left[\boldsymbol{r}_i - \boldsymbol{r}_{CM}\right]^2 \ . \tag{21}$$

where $\boldsymbol{r}_{CM}$ is the centre of mass of the polymer and

$$m = \frac{1}{M}\sum_{i=1}^{M}\left(\delta_{q_i,1} - \delta_{q_i,2}\right) \ . \tag{22}$$

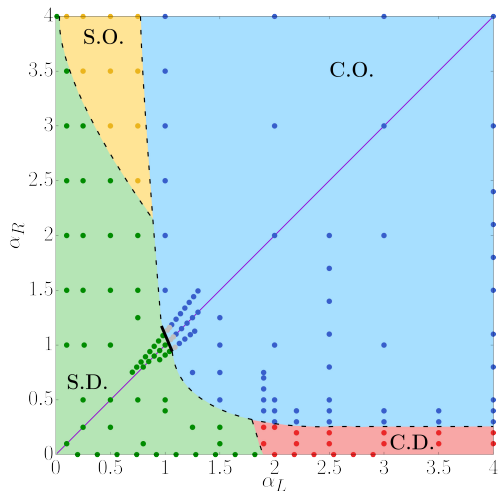

Fig. S **4**. The phase diagram of the "Potts" model in the space (α_L, α_R) for a chain with $M = 100$ beads. We can observe four different phases: (1) swollen-disordered (SD); (2) compact-disordered (CD); (3) swollen-ordered (SO); (4) compact-ordered (CO). Each dot corresponds to a set of parameters examined via an numerical simulation; grey dots represent set of parameters where coexistence between CO and SD is observed.

Phenomenology of the Potts model

The phenomenology of the model is quantified via numerical simulations at different combinations of α_L and α_R. In order to obtain enough statistics, we choose to study chains with $M = 100$ beads. We find that polymer can be found in four different phases (see phase diagram in Fig. S**4**):

(1) at small α_L and α_R values we find polymers in a *swollen-disordered* (S.D.) configuration, characterised by high gyration radius and null magnetisation;

(2) at high α_L and small α_R values we find polymers in a *compact-disordered* (C.D.) configuration, characterised by small gyration radius and null magnetisation;

(3) at small α_L and high α_R values we find polymers in a *swollen-ordered* (C.D.) configuration, characterised by high gyration radius and highly ordered spin configurations ($|m| \approx 1$);

(4) at high α_L and α_R values we find polymers in a *compact-ordered* (C.O.) configuration, characterised by small gyration radius and highly ordered spin configurations ($|m| \approx 1$).

Near the equilibrium line and at $\alpha_L \approx \alpha_R \approx 1.05$, we observe cohexistence between the C.O. and the S.D. phases, suggesting a first order phase transition (see Fig. S**5**). Note that the phase diagram and the transitions order are

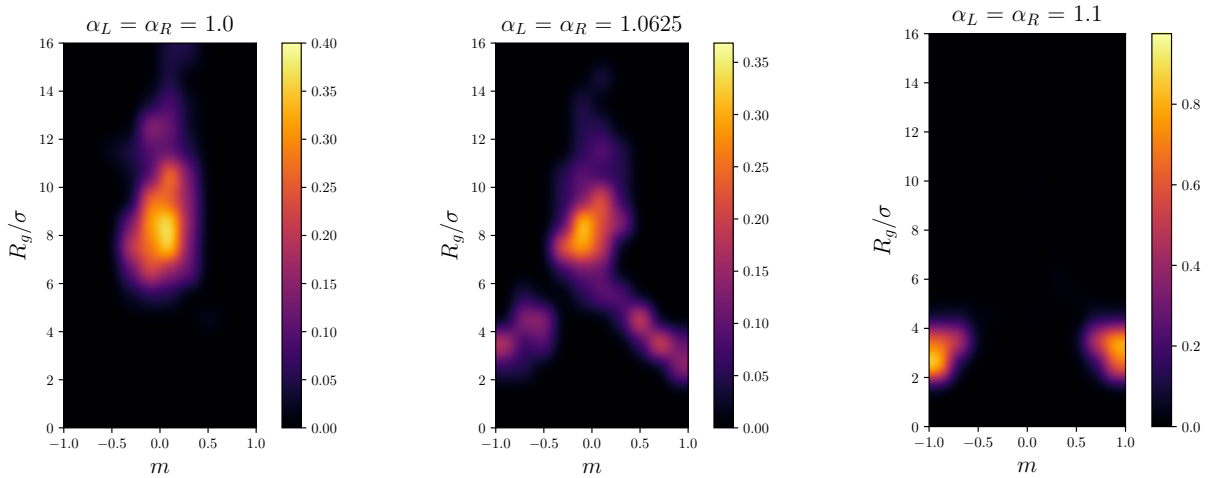

Fig. S **5**. Joint probability distributions for a chain composed of $M = 100$ beads of the signed magnetization m and the gyration radius R_g. Graphics are constructed using data obtained from 200 independent numerical simulations at the equilibrium regime ($\alpha \equiv \alpha_L = \alpha_R$) and at various temperatures ($\alpha = \{1.0, 1.0625, 1.1\}$). Note that at low temperatures ($\alpha = 1.1$) we observe the system organizes in C.O. configurations characterised by low R_g and high $|m|$. At high temperatures ($\alpha = 1$), instead, the system is in a S.D configuration, characterised by high R_g and null m. Finally, at intermediate temperatures ($\alpha = 1.0625$), we observe the coexistence between the C.O. and the S.D. configurations, suggesting the presence of a first order phase transition between these two phases.

all in great accordance to the one found in the "Voter-like" model described in the main paper.

Genomic Bookmarking in the Potts model

As discussed in the main text, we can mimic the bookmarking by imposing a fixed colour to some beads in the system. We thus consider a chain composed of M beads with fraction ϕ of bookmarks. We considered three different bookmark configurations:

(i) *Clustered* configuration: bookmarks are placed along the chain and are evenly separated, the color alternates after every n_c consecutive bookmarks;

(ii) *Mixed* configuration: bookmarks are placed along the chain and are evenly separated, the color alternates after every bookmark;

(iii) *Random* configuration: bookmarks are placed along the chain on random positions, their color is also chosen randomly between the two non-unmarked states.

As a first step we focus on the equilibrium dynamics ($\alpha_L = \alpha_R$) of a chain with $M = 1000$ beads and fraction $\phi = 0.1$ of bookmarks (total number of bookmarks $Q = \phi M = 100$). At $\alpha_L = \alpha_R = 0.98$, we find that clustered and random configurations can help the system develop long-lived compact and coherent domains, while the mixed configuration hinders the formation of ordered structures (see Fig. S**6**). Note, however, while in the Voter-like model with a random bookmark configuration we observe TAD-like formation, here only compact and block-like coherent domains are observed.

To obtain more similar result to the one showed in the main paper, we must move to a non-equilibrium dynamics. Indeed if we put the system in a region between the swollen-ordered and the compact-coherent phases (see Fig. S**7**), we observe that polymers in random bookmarking configurations develop long-lived TAD-like formations.

Replication and excision

Similarly to what done in the main text for the infection-type model. We perform simulated replication and excision also with the Potts model. As one can see from Fig. S8 the central red bookmarked region (flanked by two "non-sticky" black regions) is preserved through semi-conservative replication, whereas the rest of the polymer is flooded by blue marks which are thermodynamically preferred (here we set $\epsilon_{\text{blue}} = 1.05\epsilon_{\text{red}}$ and $\epsilon_{\text{red}} = 0.98k_BT$). In the case of replication with excision of some bookmarks (here half of the present bookmarks at each replication are removed), the red region is lost after few cell cycle. In these simulations we account for "insulating" elements such as gene deserts, but the two black segments flanking the central red bookmarked region are not required to sustain epigenetic memory (as shown in the main text).

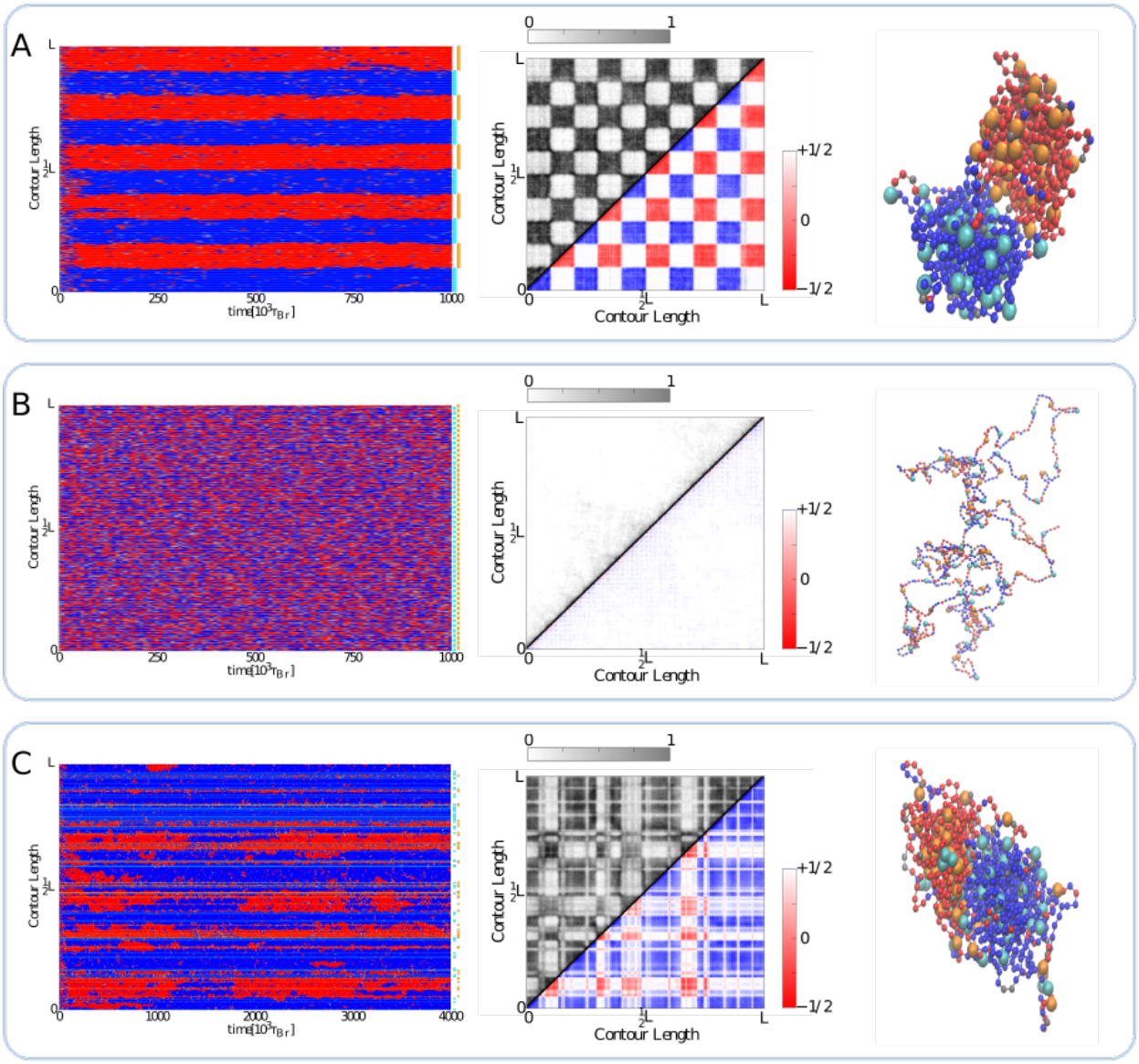

Fig. S **6**. Potts model with bookmarks: equilibrium case ($\alpha_L = \alpha_R = 0.98$). Genomic bookmarks are modelled imposing a permanent colour to certain beads of the polymer. Blue and red bookmarked beads are denoted using respectively cyan and orange colours. Plots show (from left to right) kymographs, contact maps and typical snapshots obtained via numerical simulations of polymers with $M = 1000$ beads and different bookmark configurations at $\alpha_L = \alpha_R = 0.98$. (**A**) The *clustered configuration* ($n_c = 10$) drives the polymer into two well defined compact domains. (**B**) The *mixed configuration* prevents the formation of coherent 3-d structures and the chain remains in the swollen-disordered state. (**C**) The *random configuration* can contribute to the formation of long-lived compact-coherent domains.

Drosophila simulations

We perform simulations of the Drosophila chromosome 3R with same parameters as in the Voter-like case (see above). The results are in striking agreement between the two sets of simulations, therefore strongly suggesting that the two models lead to similar behaviours at steady state (see Fig. S9).

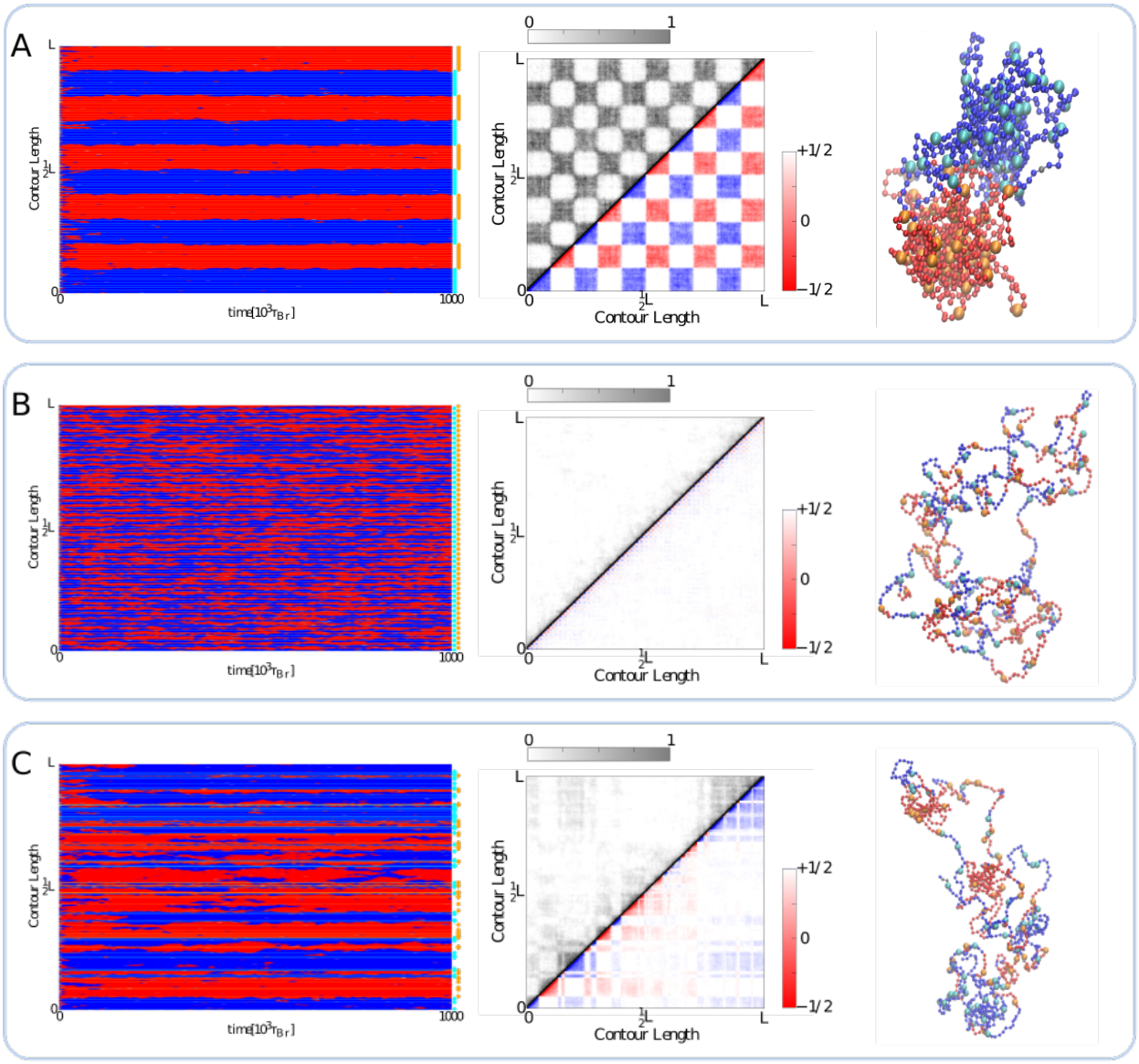

Fig. S **7**. Potts model with bookmarks: non-equilibrium case ($\alpha_L \neq \alpha_R$) Genomic bookmarks are modelled imposing a permanent colour to certain beads of the polymer. Blue and red bookmarked beads are denoted using respectively cyan and orange colours. Plots show (from left to right) kymographs, contact maps and typical snapshots obtained via numerical simulations of polymers with $M = 1000$ beads and different bookmark configurations at $\alpha_L = 0.7$ and $\alpha_R = 3$. (**A**) The *clustered configuration* ($n_c = 10$) drives the polymer into two well defined compact domains. (**B**) The *mixed configuration* prevents the formation of coherent 3-d structures and the chain remains in the swollen-disordered state. (**C**) The *random configuration* leads to the formation of TAD-like structures.

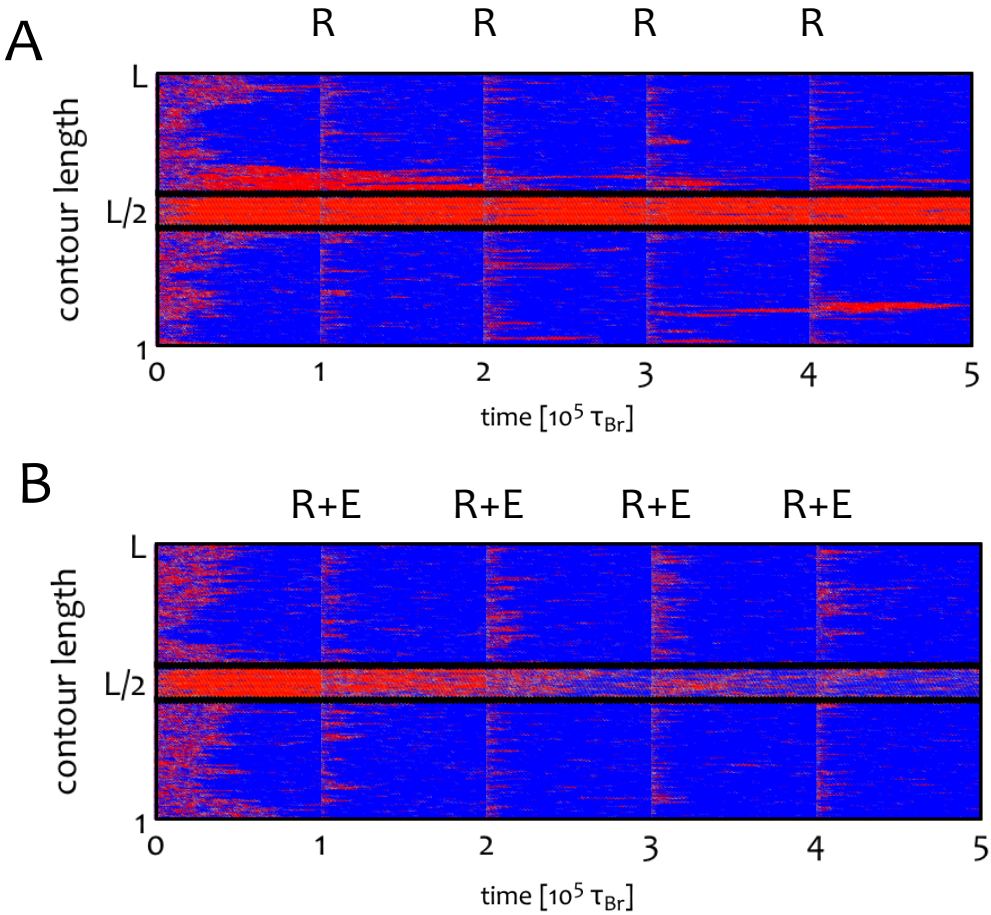

Fig. S **8**. Bookmark excision but not replication destabilises the epigenetic landscape. (**A**) Shows the case of a central red bookmarked region of a chromatin segment undergoing semi-conservative replication (R). (**B**) The same simulation, where replication is accompanied by excision (removal) of some of the bookmarks (E). Specifically we set $\epsilon_{\rm blue} = 1.05\epsilon_{\rm red}$ and $\epsilon_{\rm red} = 0.98k_BT$. The bookmarks start with density $\phi = 0.1$ within the bookmarked region and interact with other red beads and other red bookmarks with $\epsilon_{\rm red,b} = 1.2\epsilon_{\rm red}$. The black regions on either side of the red domain are "insulator" regions, made of beads which have only repulsive interactions with all other beads and cannot change their epigenetic state. These are not required to sustain the red domain but help to define its boundaries.

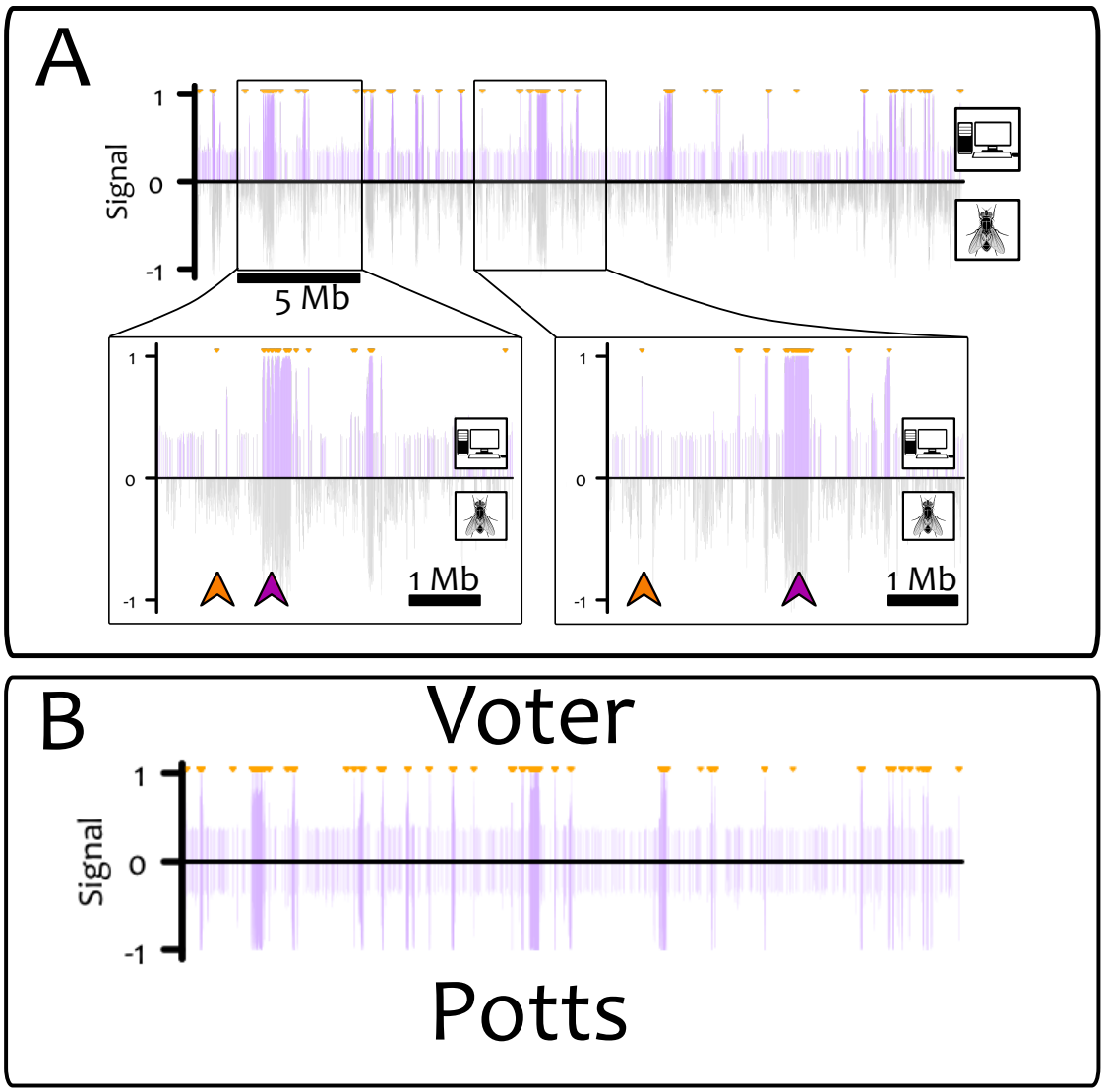

Fig. S **9**. (**A**) Comparison between in vivo (grey) and in silico (purple) ChIP-seq profiles for the H3K27me3 profile in Chr3R of Drosophila S2 cells. Here the recolouring scheme employed was the "Potts-like". (**B**) Comparison between Voter-like and Potts-like recolouring schemes. The quantitative agreement proves that at steady state the two models give very similar results.

[1] C. A. Brackley, S. Taylor, A. Papantonis, P. R. Cook, and D. Marenduzzo, Proc. Natl. Acad. Sci. USA **110**, E3605 (2013).

[2] J. Dekker, K. Rippe, M. Dekker, and N. Kleckner, Science **295**, 1306 (2002).

[3] S. Plimpton, J. Comp. Phys. **117**, 1 (1995).

[4] I. B. Dodd, M. A. Micheelsen, K. Sneppen, and G. Thon, Cell **129**, 813 (2007).

[5] D. Michieletto, E. Orlandini, and D. Marenduzzo, Phys. Rev. X **6**, 041047 (2016).